LANGMUIR

Biological and Environmental Phenomena at the Interface

Microcavity Supported Lipid Bilayers; Evaluation of Drug- Lipid Membrane Interactions by Electrochemical Impedance and Fluorescence Correlation Spectroscopy

Sivaramakrishnan Ramadurai, Nirod Kumar Sarangi, Seán Maher, Nicola MacConnell, Alan M. Bond, Dennis McDaid, Damien Flynn, and Tia E. Keyes

Langmuir, **Just Accepted Manuscript** • DOI: 10.1021/acs.langmuir.9b01028 • Publication Date (Web): 23 May 2019

Microcavity Supported Lipid Bilayers; Evaluation of Drug- Lipid Membrane Interactions by Electrochemical Impedance and Fluorescence Correlation Spectroscopy

Sivaramakrishnan Ramadurai,[1] Nirod Kumar Sarangi,[1] Sean Maher,[1] Nicola MacConnell,[1] Alan M. Bond,[2] Dennis McDaid,[3] Damien Flynn,[3] Tia E. Keyes[1]*

[1]School of Chemical Sciences and National Centre for Sensor Research, Dublin City University, Dublin 9, Ireland

[2]School of Chemistry, Monash University, Clayton, Victoria 3800, Australia

[3] Xeolas Pharmaceuticals, Dublin 9, Ireland

*Correspondence can be sent to tia.keyes@dcu.ie

Abstract

Many drugs have intracellular or membrane-associated targets thus understanding their interaction with the cell membrane is of value in drug development. Cell-free tools used to predict membrane interactions should replicate the molecular organization of the membrane. Microcavity array supported lipid bilayer (MSLB) platform are versatile biophysical models of the cell membrane that combine liposome-like membrane fluidity with stability and addressability. We used an MSLB herein to interrogate drug-membrane interactions across seven drugs from different classes, including non-steroidal anti-inflammatories; Ibuprofen (Ibu) and Diclofenac (Dic), antibiotics; Rifampicin (Rif), Levofloxacin (Levo) and Pefloxacin (Pef), and bisphosphonates; Alendronate (Ale) and Clodronate (Clo). Fluorescence lifetime correlation spectroscopy (FLCS) and electrochemical impedance spectroscopy (EIS) were used to evaluate the impact of drug on DOPC and binary bilayers over physiologically relevant drug concentrations. Whereas FLCS data revealed Ibu, Levo, Pef, Ale and Clo had no impact on lipid lateral

mobility, EIS which is more sensitive to membrane structural change, indicated modest but significant decreases to membrane resistivity consistent with adsorption but weak penetration of drugs at the membrane. Ale and Clo, evaluated at pH 5.25, did not impact the impedance of the membrane except at concentrations exceeding 4mM. Conversely, Dic and Rif dramatically altered bilayer fluidity, suggesting their translocation through the bilayer and, EIS data, showed resistivity of the membrane decreased substantially with increasing drug concentration. Capacitance changes to the bilayer in most cases were insignificant. Using a Langmuir-Freundlich model to fit the EIS data, we propose Rsat as an empirical value that reflects permeation. Overall, the data indicate that Ibu, Levo, and Pef, adsorb at the interface of the lipid membrane but Dic and Rif interact strongly, permeating the membrane core modifying the water/ion permeability of the bilayer structure. These observations are discussed in the context of previously reported data on drug permeability and Log P.

Keywords: Microcavity supported lipid bilayer (MSLB), Fluorescence lifetime correlation spectroscopy (FLCS), Electrochemical impedance spectroscopy (EIS), Lipid diffusivity, Fluorescent lifetime and Molecular brightness, Membrane permeabilization

Abbreviations: Ibu – Ibuprofen; Dic – Diclofenac; Rif-Rifampicin; ATTO – DOPE-Atto655, BODIPY – β-BODIPY-C_5-HPC; MSLB – microcavity supported lipid bilayer; FLCS – fluorescence lifetime correlation spectroscopy; EIS – electrochemical impedance spectroscopy; MH - 6-mercapto-1-hexanol; DOPC – 1,2-dioleoyl-*sn*-glycero-3-phosphocholine; DMPC – 1,2-dimyristoyl-*sn*-glycero-3-phosphocholine; τ_i – fluorescent lifetime; MB – Molecular brightness

Introduction

Irrespective of it's target, a drug must typically cross numerous membrane structures within an organism, following its administration. Understanding the extent and structural basis of interaction of pharmaceuticals with the lipid membrane is crucial in drug discovery as such information can aid in predicting membrane permeability or membrane-associated toxicity during the design of drugs with intracellular targets.[1–3] The cellular membranes are semi-permeable barriers comprised of complex matrices of the phospholipid bilayer, sterol and associated membrane proteins. Many drug molecules have intra-cellular targets. The alterations such species impose on membranes as they associate with and permeate these dynamic structures can have a profound influence on membrane structure, such as thickness, curvature, permeability and fluidity.[4,5] And, can affect biological function including the integrity of the membrane barrier effect, cell signaling and adhesion, and thus in the toxicity of the drug.[6–9] For example, anesthetic molecules such as chloroform, halothane and diethyl ether have been shown to induce lateral expansion in the membrane, increasing local disorder in lipid tails adjacent to the intercalating anesthetic molecule.[10] Similarly, amphotericin B, an antifungal agent, disrupts the fungal cell wall by making pores on the membrane that lead to cell death.[11–13] Valinomycin and gramicidin A (gA) permeate the bilayer by forming ion channels that alter the membrane electrochemical resistivity.[14–16]

Molecular lipophilicity is one of the key physicochemical properties considered predictive of passive molecular diffusion across the biological membrane[17]. Log P is one of the most commonly used reference systems for the assessment of molecular lipophilicity and prediction of permeability. Where P is the partition coefficient of a neutral molecule between an aqueous and lipophilic (usually octanol) phase. For ionized species the distribution coefficients, $LogD$, the ratio of the sum of the concentrations of ionized and unionized forms of the compound in two phases is more appropriate.[11] Though widely used in the pharmaceutical industry, these parameters are fairly crude predictors of membrane association and permeability that provide limited insight into the molecular nature of drug-membrane interaction. Indeed, recent evidence indicates that not only hydrophobicity but also lipid composition plays an important role in the passive diffusion of drugs across the lipid bilayer.[4,18,19]

Artificial membranes offer a valuable means to study the interactions of drugs with the membrane during the earliest stages of drug development and can be used to anticipate both passive membrane permeability and membrane associated toxicological problems isolated from the complexity of the living cell.[20] Also, where the molecular target is a membrane protein or where permeation is mediated through protein interaction, molecular insights into membrane-molecular interactions are important. Various biomimetic models such as liposomes and supported lipid bilayers (SLB) methods are widely used to

interrogate the behavior of membrane lipids with small molecules. However, undulation of the membrane, limited stability, compositional versatility and means of interrogation are drawbacks attributed to unilamellar vesicles. Whilst, interference from the interfacial support on the fluidity and functionality of the bilayer and associated proteins in SLBs, are limitations to the application of these models in study of lateral diffusion of proteins and lipids in the membrane.[21,22] Several modifications have been introduced to improve fluidity in supported membrane models, including tethered lipid bilayer membranes and cushioned bilayer membranes,[23] but the lateral mobility of lipids and reconstituted proteins typically do not attain the mobility reported for giant unilamellar vesicles. Alternative approaches have emerged that assemble membranes supported over pores which can improve fluidity whilst maintaining stability.[24–26] We recently reported a microcavity supported lipid bilayer (MSLB) formed from polystyrene sphere templated polydimethylsiloxane (PDMS)[27] for optical measurements and on gold-coated silicon wafers for electrochemical measurements. These platforms, because of their aqueous filled pore underlying the bilayer, combine the fluidity of a liposome with stability and versatility reminiscent of an SLB. These properties, along with their ease of interrogation by electrochemical and optical microscopy means and the deep aqueous reservoir below their proximal lipid leaflet make the MSLBs a versatile platform for interrogating molecular -membrane interactions at a lipid bilayer membrane in a robust, relatively quick and facile manner.

Herein, using MSLB platforms, we examined the interactions of seven well-characterized drugs with biomembranes from three different families; non-steroidal anti-inflammatories; Ibuprofen (Ibu) and Diclofenac (Dic), antibiotics; Rifampicin (Rif), Levofloxacin (Levo) and Pefloxacin (Pef), and bisphosphonates; Alendronate (Ale) and Clodronate (Clo)., selected because they span different solubility, $Log\ P$ and apparent permeability coefficients (P_{app}). The concentration of the drugs incident at the microcavity supported lipid bilayer was systematically varied and fluorescence lifetime correlation spectroscopy (FLCS) was used to evaluate and compare the changes in the lateral mobility, fluorescence lifetime (τ_i) and molecular brightness (MB) of lipid probes in the membrane in response to drug concentration. In parallel, electrochemical impedance spectroscopy (EIS) was used to evaluate changes to membrane thickness and permeability as a function of drug concentration. Our data show significant and consistent changes on membrane interactions with drug type and provide new insights into drug-membrane behavior. The study indicates that the microcavity SLB platform is a useful and versatile interrogative tool for understanding and evaluating drug-lipid membrane using interactions.

Materials and Methods

Materials

1,2-Dioleyl-*sn*-glycerophosphocholine (DOPC), 1,2,-Dioleyl-*sn*-glycerophosphoethanolamine (DOPE), 1,2,-Dioleyl-*sn*-glycerophosphoserine (DOPS), and 1,2,-Dioleyl-*sn*-glycerophosphoglycerol (DOPG) in powder form were purchased from Avanti polar lipids (Instruchemie, The Netherlands). Ibuprofen (Ibu), Diclofenac (Dic) sodium salt, Levofloxacin, Pefloxacin, Rifampicin, Alendronates, Clodronates and phosphate buffer saline (PBS) tablets were purchased from Sigma-Aldrich (Wicklow, Ireland), β-BODIPY-C_5-HPC ((2-(4,4-Difluoro-5,7-Dimethyl-4-Bora-3a,4a-Diaza-s-Indacene-3-Pentanoyl)-1-Hexadecanoyl-sn-Glycero-3-Phosphocholine) (530/550nm) was purchased from Thermofisher (Ireland) and DOPE-atto655 (ex. 650/em. 670nm) was purchased from Atto-tech GmbH (Siegen, Germany). All other chemicals were of HPLC grade from Sigma-Aldrich (Wicklow, Ireland), and were used as purchased. Ultrapure water with a resistivity ≥ 18.2 MΩcm was produced by a MilliQ (Millipore Academic) system and used for buffer preparation.

Vesicle preparation

The one component, binary and ternary lipid mixtures were prepared from DOPC, DOPC:DOPG (3:1), DOPC:DOPS (3:1), DOPC:DOPG:DOPE (2:1:1), [mol:mol]. For FLCS, lipids and fluorescent lipid probe (β-BODIPY-C_5-HPC (BODIPY) and DOPE-Atto655 (ATTO)) were mixed in a ratio of 10000:1 mol/mol and dried under vacuum. The dried lipid films were rehydrated in 1 ml of 0.01 M phosphate buffer saline (PBS), pH 7.4 or 0.02 mM Tris buffer, pH 5.25 and vortexed for a period of 30-60 s. Next, the lipid suspensions were extruded 11 times through a 100 nm polycarbonate filter using a mini-extruder (Avanti Polar Lipids) to form large unilamellar vesicles (LUV) that were then diluted to final concentration of 0.25 mg/ml and stored at 4 °C for further use. The vesicles were prepared in the same way but without the fluorescent probe for EIS measurements.

Microcavity array supported lipid bilayers

Lipid bilayers were suspended across aqueous filled microcavity arrays according to protocols modified slightly from previous reports.[27,28] For fluorescence studies the microcavity arrays were made from polydimethylsiloxane (PDMS) [Sylgard 184 base and curing kit, Dow Corning]. Briefly, PDMS was cast onto a dried film of polystyrene spheres of 2.88 μm diameters, formed on freshly cleaved mica, and cured. The PDMS was peeled off the mica and the spheres were removed to form open spherical cavities embedded in PDMS. The planar PDMS was plasma cleaned, followed by 1 h of sonication in PBS buffer to ensure the cavities were filled with the aqueous solution.

Following aqueous filling, a combination of Langmuir-Blodgett (LB) and vesicle fusion (VF) methods were employed to fabricate MSLB. The details of Langmuir-Blodgett techniques are described in supplementary information. The microcavity for EIS measurements was made in an analogous way at gold-coated silicon wafers and the details are described in SI.

Fluorescence Lifetime Correlation Spectroscopy (FLCS)

FLCS experiments were performed using a Microtime 200 system (PicoQuant GmBH, Germany) consisting of FCS module, dual SPD detection unit, time-correlated single photon counting (TCSPC), and inverted microscope model Olympus X1-71 with a Olympus UPlan SApo 60x/1.2 water immersion objective. The lipid labeled fluorophores BODIPY and ATTO were excited using pulsed picosecond lasers at 532 nm laser PicoTA from Toptica (Picoquant) and 640 nm LDH-P-C-640B Picoquant, respectively. A single mode optical fiber guides the two lasers to the main unit and provides a homogeneous Gaussian profile for both excitations. The lasers were pulsed at 20 MHz, corresponding to an interval of 50 ns. The emitted fluorescence was collected through the microscope objective and dichroic mirror z532/635rpc blocked the backscattered light and HQ550lp AHF/Chroma for 532 nm and HQ670lp AHF/Chroma for 640 nm filters were used to clean up the signal. A 50 μm pinhole was used to confine the volume of detection in the axial direction. Fluorescence was detected using a single photon avalanche diode (SPAD) from MPD (Picoquant). The time-correlated single photon counting system (PicoHarp 300 from Picoquant), enabled simultaneous assessment of the lifetime in a nanosecond range along with the time of diffusion in the millisecond range.[58] Using TCSPC allowed us to filter any contribution from after-pulsing, suppress scattered light and parasitic signals and background,[30,31] and in parallel to calculate the fluorescence lifetime of the lipid probes in situ.

To calibrate the FCS confocal volume, Rhodamine 6G (532nm) and Atto655 (640nm) dyes with known diffusion coefficients were used.[32] The volume was determined at the start of each set of experiments and at least 15 data points were collected from each sample and each data point was measured for 30 sec. The time-dependent fluctuations of the fluorescence intensity d$I(t)$ were recorded and analyzed by an autocorrelation function $G(t)= \mathrm{I} + \langle \mathrm{d}I(t') \, \mathrm{d}I(t'+ t)\rangle / \langle I(t')\rangle^2$. As has been shown theoretically for an ensemble of m different types of freely diffusing species, $G(t)$ has the following 2-dimensional analytical form:[33]

$$G(t) = 1 + \left[1 + \frac{f_T}{1 - f_T} e^{-t/\tau_T} \right] \frac{1}{\langle N \rangle} \sum_{i=1}^{m} \left(1 + \left(\frac{\tau}{\tau_{D_i}} \right)^{\alpha} \right)^{-1} \qquad (1)$$

Here <*N*> is the average number of diffusing fluorescence species in the observation volume, f_T and τ_T are the fractions and the decay time of the triplet state respectively, τ_{Di} is the diffusion time of the ith species, and α is the anomalous exponent respectively. α indicates the extent of deviation of diffusion coefficient (*D*) from Brownian behavior and it can vary between 0 to 2. A value of 1 indicates the free diffusion.[34,35] The experimentally obtained $G(t)$ is fit equation (1), to yield the diffusion time, τ_{Di} which is related to the diffusion coefficient *D* through $D = r_0^2/4\tau_{Di}$, where r_0 is the lateral radius of the confocal volume. The fits of the autocorrelation curves were carried out using the PicoQuant software package using a least square Marquard-Levenberg algorithm.

The fluorescent decays were fit to a multi-exponential model to obtain the luminescent lifetime, τ_i of the probe according to equation 2.[36]

$$I(t) = \sum_{i=1}^{n} a_i \, exp\left(-t/\tau_i\right) \qquad (2)$$

where τ_i are the lifetimes with amplitudes a_i. The values of τ_i and a_i were determined using PicoQuant Symphotime software with nonlinear least-square fitting.

The Molecular Brightness (MB) was calculated by dividing the average photon-counts per second by average number of molecules (N) computed from equation 1, given below[37,38]

MB [counts per second per molecule] = <Average photon-counts>/ <N>

All measurements were performed at 20 ± 0.4 °C.

Electrochemical Impedance Spectroscopy, EIS.

EIS was performed with a CH660A potentiostat (CH Instruments, USA). A standard 3-electrode cell was employed which are comprised of an Ag/AgCl (1M KCl) reference electrode, a platinum wire auxiliary electrode and the gold microcavity array which constituted the working electrode. The EIS data were measured over a frequency range of 0.01 to 10^4 Hz with an ac modulation amplitude of 0.01 V at a potential bias of 0 V (vs Ag/AgCl). All measurements were carried out in a glass cell (approximate volume of 4 ml) in contact with electrolytes PBS buffer maintained at pH 7.4 or 20 mM Tris buffer at pH 5.25. The EIS of the aqueous filled microcavity array coated with the lipid bilayer was measured initially prior to addition of drugs to ensure signal stability. Subsequently, drug solutions were titrated into the glass cell containing buffer and the electrochemical impedance response of the lipid bilayer measured for each concentration. Each measurement takes approximately 10 min and were carried out at room temperature (20 ± 0.4 °C). The measured data were analyzed using Z-View software with the fitting model (Scheme 1) to determine the changes in membrane resistivity and conductance on drug interaction.

Equivalent circuit model for MSLB

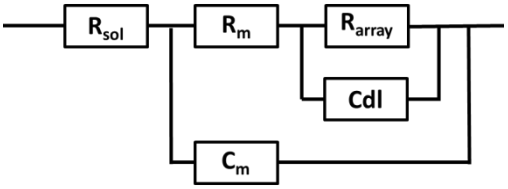

Scheme 1: ECM model used to fit EIS data.

In order to extract the resistance and capacitance values for the MSLBs, the EIS data were fit to the equivalent circuit model (ECM) shown in scheme 1 which was described previously for the lipid bilayer modified microcavity array electrode.[10] The circuit consists of the solution resistance (R_{sol}) in series with a resistor and a capacitor, which are in parallel and correspond to the electric and dielectric properties respectively of membrane deposited on the electrode surface (R_m, C_m). The ECM also contains an additional component to account for the resistance of the cavity array (R_{array}), and the double layer capacitance (C_{dl}). The data for the bare cavities and those treated with MH were fitted with a R_{sol}(Rm||Cm), true constant as at this stage, as in the absence of the bilayer, the resistance and capacitance are expected to be uniform along the surface of the electrodes. A Constant Phase Element (CPE) is used in the equivalent circuit instead of pure capacitors to account for surface defects on both the electrode surface and the lipid bilayer. The impedance of a CPE is given by $Z_{CPE} = Q^{-1}(j\omega)^{-\beta}$ where Q is the magnitude of the capacitance of the CPE, ω is the angular frequency, and β is a real number between 1 and 0 (the closer β approaches 1, the more ideal the capacitive behavior of the CPE).

Langmuir and Langmuir-Freundlich Isotherms

The EIS data for each drug were iteratively fit to non-linearized Langmuir and Langmuir-Freundlich isotherm expression as defined by Eq. (3) and (4) respectively;[39]

$$\Delta R = \frac{R_{sat}(K_a C)}{1 + K_a C} \qquad (3)$$

$$\Delta R = \frac{R_{sat}(K_a C)^n}{1 + (K_a C)^n} \qquad (4)$$

where ΔR is the change in membrane resistance, as function of bulk drug concentration, R_{sat} is absorption capacity that relates to the number of available binding sites, K_a is affinity constant for adsorption, C is the equilibrium concentration of the drugs and n (dimensionless) is the index of heterogeneity.

Results

Figure 1 shows a schematic representation of the MSLB platform preparation used in this work For fluorescence measurements, a microsphere templating method reported previously[27] was used to prepare PDMS microcavity arrays and is described in the methods section. The fluorescently labeled bilayers were suspended across the aqueous filled microcavity array by a combined LB-VF method, as illustrated in Fig. 1.

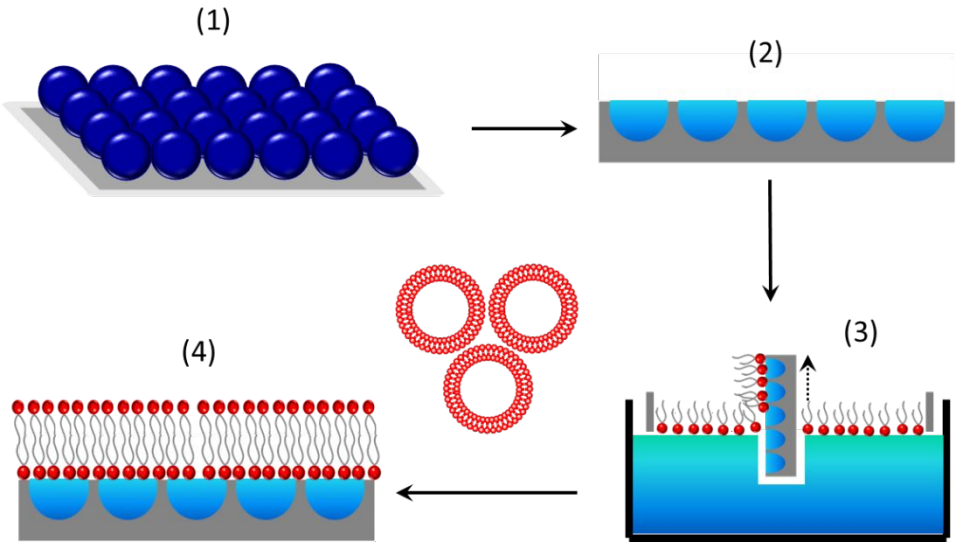

Figure 1: A representation of MSLB platform preparation. (1) The polystyrene beads of diameter 2.88 μm were drop cast either on a gold-coated silicon wafer for EIS or on mica for FLCS measurements, (2) Formation of microcavities on gold using electrodeposition method and on PDMS by a solidifying method. (3) Microcavities were filled with buffer and form a lipid monolayer using the Langmuir-Blodgett technique. (4) Lipid vesicles, with fluorescent lipid probes for FLCS, were allowed to disrupt on the lipid monolayer to form the bilayer. Microcavity made on PDMS, turned into a small portable microfluidic device for FLCS measurement.

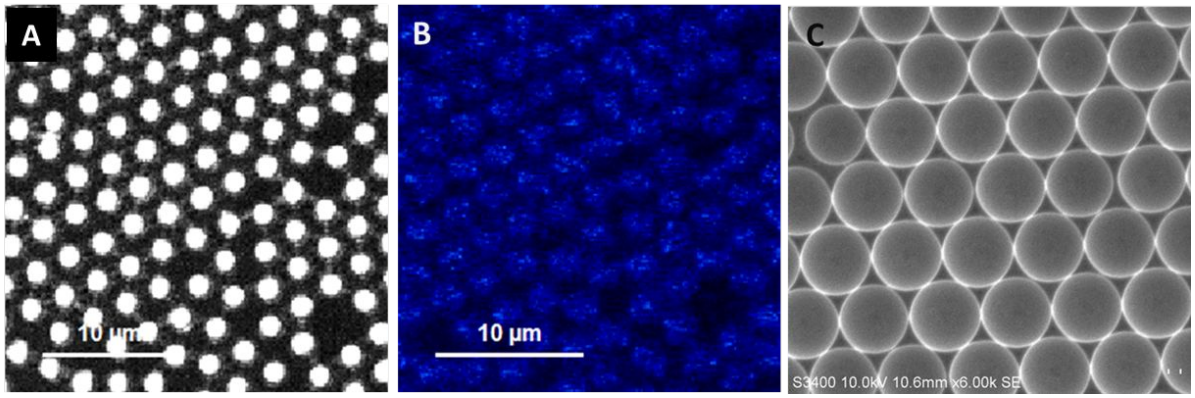

Figure 2: Representative microcavity array formed on PDMS and gold substrate. (A) Reflectance image acquired from confocal microscopy, where the white spot represents an aqueous filled cavity and the black area corresponds to planar and unfilled cavities. (B) Fluorescent image of lipid bilayer labeled with DOPE-Atto655 spread across the microcavity array to form MSLB using the LB-VF method. (C) Scanning electron microscopy image of microcavity array formed on the gold substrate using the electrodeposition method. The scale bar was 10 µm.

The refractive index mismatch between PDMS (n ~ 1.45) and the buffer (n ~ 1.33) enables precise location of the pore suspended bilayers as the aqueous filled pores appear as intensely reflective spots in the white light back reflectance images as shown in Figures 2A and B. On locating the spanning bilayer, the observation volume is positioned at the center of a micropore and the bilayer located by z-scanning to find the most intense fluorescence point from where the autocorrelation function (ACF) trace is then collected. Time traces were, in all cases, acquired for 30 s and SymPhoTime 64 software was used to acquire and analyze the time traces. Representative ACF curves for labeled lipid diffusion in DOPC over a cavity are shown in Figure 3 (*vide infra*) along with their fit to the 2D-diffusion model (equation 1). The calculated diffusion coefficient of DOPE-ATTO655 in DOPC lipid membrane is 11.7 ± 0.47 $\mu m^2 s^{-1}$ and that of β-BODIPY-C5-HPC, 14.20 ± 0.8 $\mu m^2 s^{-1}$. These values are consistent with reported literature diffusion coefficient values for these probes at microcavity suspended bilayers as well as giant unilamellar vesicles (GUVs),[27,40,41] and reflect the high degree of fluidity of the lipids supported across the aqueous filled micropores.

For EIS studies, the microcavities were prepared by polystyrene sphere templating and electrodeposition of gold onto gold-coated silicon wafers as reported previously [14,28] and the step by step protocol is also presented in experimental methods. Figure 2C shows a representative SEM image of the working area of the electrode. Such images confirm that the gold electro-deposition technique implemented produced uniform areas (~1 cm^2) of ordered closely packed 2.80 ± 0.04 µm microcavity arrays. The impedance of

the bilayer was monitored over 8 h to confirm that the impedance signal and thus the membrane is stable with no spontaneous changes to EIS signal observed during the experimental time window (cf. Fig. S1 and Table S1, supplementary information (SI))

Drug-Membrane Interactions

NSAIDs: Ibuprofen and Diclofenac

The impact of Ibu on the fluidity of a DOPC lipid bilayer membrane was examined by systematically varying the concentration of Ibu from 1 μM to 1 mM. This concentration range was selected to encompass the reported therapeutic blood plasma levels of Ibu which lie in the range of 2 - 40 μM with higher concentrations lying the range present in the gastrointestinal (GI) tract.[42–44] Ibu in PBS buffer was injected into the flow chamber and allowed to equilibrate for 10 mins with the DOPC MSLB. Control experiments where the equilibration times were extended over an hour confirmed no further changes to lipid mobility occurred beyond 10 mins. To build statistical significance, ACFs were collected from between 20 and 30 different micropores across a single substrate. ATTO655-DOPE (ATTO) and β-BODIPY-C_5-HPC (BODIPY) were both used to probe the different aspects of the membrane environment. The ATTO is a cationic oxazine probe, which is relatively hydrophilic and conjugated to the lipid headgroup so resides at the aqueous interface of the lipid bilayer. Conversely, BODIPY is a hydrophobic probe, expected to orient relatively deeply into the hydrophobic core of the bilayer. These probes are well suited for FCS studies due to their high photostability and quantum yields.[45] Figures 3A and B show representative ACF curves for ATTO and BODIPY lipid probes at DOPC MSLBs respectively following addition to 400 μM of Ibu. The resulting data, following curve fitting to equation (1), is shown in the supplementary information (Table S2a,b, SI). FLCS enables us to simultaneously measure the fluorescence lifetime of the lipid probe along with FCS data. The molecular brightness (MB) of the lipid probe in the membrane as a function of Ibu concentration also was calculated.

The diffusion coefficients of the ATTO probe across the different drug concentrations were, within experimental error, unaffected by bilayer exposure to Ibu (Table S2a, SI). The fluorescence lifetime of ATTO in the DOPC MSLB was 3.3 ± 0.02 ns with an MB of 6300 ± 600 counts per seconds per molecule (cpsm); both parameters were similarly unaffected by the presence of Ibu in the contacting medium. As expected, α values for diffusion of the lipid probe both in the absence and across all the concentrations of Ibu were 0.98 ± 0.02, reflecting Brownian diffusion of ATTO in DOPC membrane.

The diffusion coefficient of BODIPY in the DOPC bilayer was found to be 14.20 ± 0.8 $\mu m^2 s^{-1}$ and although only slightly dependent on Ibu concentrations, at the highest Ibu concentration (1000 μM) *D* had

decreased to 12.40 ± 0.7 $\mu m^2 s^{-1}$ (Table S2b, SI). The BODIPY probe exhibits faster diffusion than the ATTO. The fluorescence lifetime of BODIPY obtained in our studies is comparable to reported values in unilamellar vesicles and in methanol.[30,46] The α value for this probe was 0.98 ± 0.01 consistent again with normal Brownian diffusion and similarly, no significant changes to diffusion modality were observed upon addition of Ibu to the contacting media. The fluorescent lifetime of the BODIPY probe was 5.94 ± 0.08 ns for DOPC alone and this decreased modestly to 5.83 ± 0.03 ns when the bilayer was in contact with Ibu concentrations exceeding 100 μM. The MB of BODIPY was unaffected by increasing concentrations of Ibu and measured as 12700 ± 1100 cpsm. Thus we conclude from FLCS that introduction of Ibu has modest impact on the fluidity or viscosity of the DOPC lipid membrane.

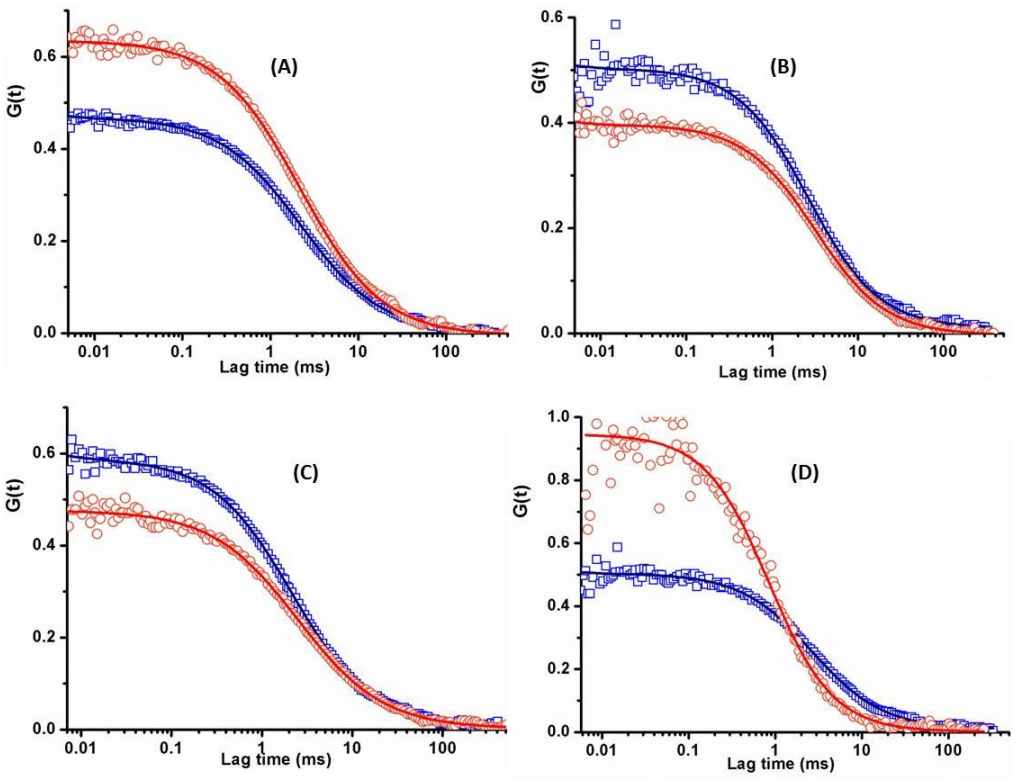

Figure 3: Representative ACF data for (A) Ibuprofen BODIPY, (B) Ibuprofen ATTO, (C) Diclofenac BODIPY, (D) Diclofenac ATTO in DOPC lipid membrane on PDMS microcavity as a function of (□) 0 and (○) 400 μM of drug concentration. The lipid membrane suspended across the 2.88 μm cavity was filled with the PBS buffer, pH 7.4. 532 nm and 640 nm pulsed lasers were used to excite the BODIPY and ATTO molecules.

Next, we studied the interaction of Dic with the DOPC lipid bilayer under the same conditions and concentrations used for Ibu, as their physiological concentrations are the same.[47] Figures 3C and D show representative ACF data for DOPC MSLB labeled with BODIPY and ATTO lipid probes respectively

before and after 400 μM Dic. Whereas, as reflected in Figures 3C and D, changes in the ACF data for the BODIPY labeled DOPC bilayer were modest, systematic concentration-dependent changes were observed for the ATTO labeled membrane. Tables 1 and S3 (SI) show the outcome of the fitting of FLCS data for ATTO and BODIPY labeled DOPC lipid membranes against the Dic concentrations. The *D* value of ATTO-DOPE in DOPC bilayer alone was 11.7 ± 0.47 $\mu m^2 s^{-1}$ and this was unchanged at the lowest concentrations of Dic (1 and 4 μM). However, *D* dramatically rises to 43.5 ± 4.7 $\mu m^2 s^{-1}$ for 800 μM and 1000 μM (Table 1). The number of molecules (*N*) in the observation volume was reduced from 3 for DOPC MSLB in the absence of Dic to 1 at higher concentrations of Dic (Table 1). Interestingly, the α value for ATTO was also influenced by Dic where it increased from ~ 1 for DOPC bilayer alone/lower Dic concentrations to 1.21 ± 0.09 for concentrations of Dic exceeding 10 μM. The fluorescence lifetime of ATTO in DOPC lipid bilayer was reduced from 3.3 ± 0.02 ns to 2.44 ± 0.06 ns with increasing concentration of Dic in the contacting solution. Similarly, MB of the ATTO in DOPC lipid bilayer was reduced from 6300 ± 600 cpsm in the absence of Dic to 1000 ± 100 cpsm for 1 mM of Dic concentration in the contacting solution. At the end of the titration, the membrane contacting buffer was exchanged for fresh PBS buffer to remove the drugs from the contacting solution. Following this treatment the *D* value of ATTO reduced to 22.0 ± 2.0 $\mu m^2 s^{-1}$ but did not fully recover, suggesting Dic irreversibly associated or permeates the membrane.

Table 1: FLCS determined parameters of ATTO lipid probes in the DOPC lipid membrane at designated doses of Dic in PBS buffer, pH 7.4.

Conc. (μM)	Mol. Brightness (X 1000)	Fluor. lifetime (ns)	Anomalous exponent α	N	D ($\mu m^2/s$)
0	6.3 ± 0.6	3.3 ± 0.02	0.98 ± 0.02	3.0 ± 0.5	11.7 ± 0.47
1	6.2 ± 0.5	3.3 ± 0.01	1.05 ± 0.02	2.5± 1	13.7 ± 0.3
4	6.1 ± 0.5	3.28 ± 0.01	1.0 ± 0.02	3.5 ± 0.5	11.9 ± 0.75
10	6.2 ± 0.4	3.24 ± 0.01	1.15 ± 0.02	2.0 ± 0.5	16.6 ± 0.8
40	5.0 ± 0.4	3.16 ± 0.01	1.08 ± 0.03	1.5 ± 0.5	18.0 ± 1.2
100	3.9 ± 0.5	3.04 ± 0.01	1.19 ± 0.04	1.0 ± 0.2	24.0 ± 2.4
400	1.6 ± 0.2	2.78 ± 0.04	1.21 ± 0.06	1.0 ± 0.4	34.3 ± 3.0
800	1.1 ± 0.1	2.5 ± 0.07	1.16 ± 0.5	1.0 ± 0.5	43.5 ± 4.7
1000	1.0 ± 0.1	2.44 ± 0.06	1.21 ± 0.09	1.5 ± 0.5	41.5 ± 5.0
After wash	6.0 ± 0.5	3.15 ± 0.02	1.14 ± 0.02	1.5 ± 0.5	22.0 ± 2.0

As a control measure, we introduced Dic at random concentrations to the bilayer and subsequently removed the drug from the contacting solution and measured the changes using FLCS (Table S4, SI) to preclude the possibility that changes observed in the membrane are due to systematic damage to the bilayer caused by long exposure time to Dic. As shown in Table S4 (SI), the changes in the membrane dynamics either due to systematic titration of Dic or random addition of drug led to the same numerical values at each concentration point. This result indicates that Dic binds irreversibly to the membrane in a concentration-dependent manner where it impacts on the diffusion of ATTO which is oriented at the membrane aqueous interface. The behavior of the ATTO probe, its increasing diffusion coefficient and the anomalous exponent is similar to behavior observed when PEG was used to treat the DOPC bilayer.[48] We had attributed this behavior to the association of the ATTO probe with the bound interfacial PEG and its localization at the membrane interface. Here, the changes are only observed at concentrations of Dic exceeding 10 μM. We speculate that the opposing charges at the ATTO and Dic adsorbed at the bilayer interface lead to electrostatic interactions between the two, leading to the association of the ATTO with the Dic at the bilayer interface.

We then examined the impact of Dic on BODIPY diffusion as this uncharged species orients within the bilayer core. The ACF fits for diffusion of BODIPY are tabulated in Table S3, SI. The diffusivity was observed to decrease slightly following the introduction of the drug, from 14.2 ± 0.8 $\mu m^2 s^{-1}$ for the DOPC in the absence of Dic to an average D value of 12.27 ± 0.75 $\mu m^2 s^{-1}$ for 1, 4, 10 and 40 μM of Dic (Table S3, SI). Although this change was minimal relative to standard error, the mean trend was highly consistent across all replicates. The diffusivity decreased further to 11.44 ± 0.8 $\mu m^2 s^{-1}$ at Dic concentrations exceeding 100 μM. Unlike ATTO, the N and α values were unaffected by the presence of Dic, whereas the τ_i and MB of the BODIPY in DOPC lipid bilayer decreased upon increasing the concentration of Dic in the contacting solution (Table S3, SI). The lifetime of the BODIPY label within the bilayer was 5.94 ± 0.08 ns in the absence of Dic and systematically decreased with increasing Dic concentration to 4.12 ± 0.03 ns at 1 mM Dic concentration. Correspondingly, the MB value of the probe decreased from 12700 ± 1100 cpsm for DOPC to 3400 ± 400 cpsm for 1 mM Dic concentration. To exclude the possibility of Dic interaction with BODIPY that leads to the reduction of its lifetime (τ_i), we independently measured the τ_i of BODIPY in chloroform : methanol (1:1) solution in the absence of bilayer. Upon introducing different concentrations of Dic upto 1mM, no change in the lifetime of the probe was detected compare to the untreated solution (Table S5, SI) suggesting the change in τ_i only occur in the membrane and not in solution. Taken together, the data indicate penetration of the Dic into the hydrophobic core of the membrane. The modification to florescence lifetime and molecular brightness indicate a change in the probes environment which can only occur if the Dic is penetrating the

hydrophobic core and suggests taken with the irreversibility of the response at the ATTO probe that Dic permeates the membrane. Finally, we introduced fresh PBS buffer to the MSLB to remove the drug from the contacting solution and acquired ACF data for the probe in the membrane. As observed for the ATTO labelled bilayer D, τ_i and MB only partly recovered indicating Dic remains bound, penetrating the hydrophobic core of the membrane (see after wash in Table S3, SI).

EIS was then used to evaluate the impact of Ibu on changes in resistance and capacitance of lipid bilayer as this method is expected to be highly sensitive to ion permeation or modifications to bilayer packing or thickness if induced by the drug. The Ibu sodium salt in PBS buffer was introduced to the contacting solution of a DOPC bilayer on a gold microcavity, which functioned as the working electrode under the same conditions as described for the FLCS studies. The membrane resistance of the bilayer was evaluated prior to addition of the drug and found to be 5.56 ± 0.23 MΩcm^2 (cf. Fig. S1 and Table S1, SI), which is consistent with the reported values for other SLBs based on either DOPC and/or different lipid compositions which are typically in the range of 0.1 to 4 MΩcm^2,[14,21,23,49–52] depending on the modification of electrode surface and surface area.

The Ibu concentration was systematically increased from 1 μM to 4 mM, where the cavity was filled with PBS buffer at pH 7.4 (Table S6, SI). Equilibration time was 10 mins after each concentration increase before EIS was measured, as before controls indicated no further change beyond this time interval. Data were measured for each drug concentration in triplicate. There was no variation in response over these triplicate measurements again, confirming equilibrium between the drug and membrane occurred quickly. Each EIS measurement took 10 min to complete and the repeat measurement was taken directly after the preceding measurement. Then, after the highest concentration had been introduced, allowed to equilibrate, and EIS measured in triplicate, the lipid bilayer was washed through twice with PBS buffer to clear any remaining drug from the contacting solution. This was carried out to assess the reversibility of drug binding. In a separate EIS control experiment, we confirmed that exchanging the bilayer contact solution in this way had no measurable impact on the bilayer impedance.

Figure 4A shows a representative Nyquist plot of the complex impedance data for a single DOPC lipid-MSLB with variable concentrations (0, 40, 400, 100 μM) of Ibu. For a Nyquist plot, the sum of the real, Z', and imaginary, Z'' components represents the complex impedance (Fig. 4) which originates from the resistance and capacitance of the cell. An EIS data shifts towards Z'' (y-axis), indicates that there is an increase in the impedance of the bilayer. Similarly, a shift towards Z' (x-axis) implies that the bilayer impedance is reduced. In lipid bilayer systems, reduced impedance (or admittance) is typically attributable to increased permeability or membrane ionic/aqueous leakiness,[53] i.e. reduced electrochemical

resistance arising typically from changes to lipid packing or ion permeability. From visual inspection of the EIS curves, it is evident that Ibu causes a small but systematic decrease on bilayer impedance, as illustrated in Figure 4A. For quantitative insight, we extracted the resistance values of the lipid bilayer by fitting the EIS data to the equivalent circuit model (ECM) shown in Scheme 1. The relative change in resistance and capacitance values before and after drug addition, the data extracted from the fit results are summarized in Table 2.

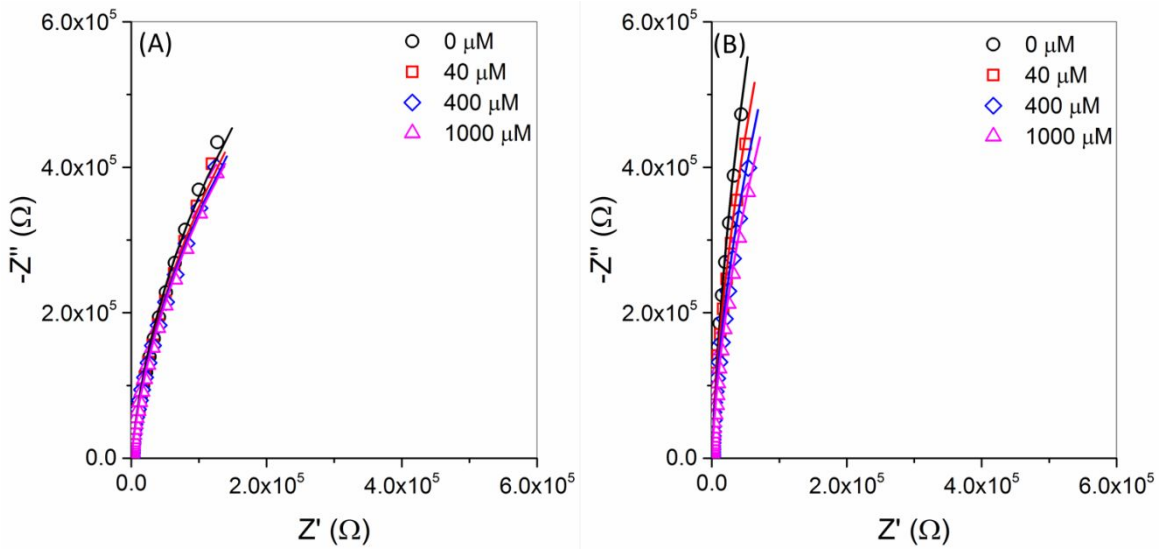

Figure 4: Nyquist plot titration of Ibu and Dic drugs into contacting solution at a DOPC bilayer suspended across 2.88 μm cavities in a 0.01 M PBS solution (pH 7.4): frequency range 0.01 Hz to 10^4 Hz with a bias potential of 0.0 V vs Ag/AgCl (1 M KCl). The ○, □, ◊, Δ symbols represent DOPC lipid bilayer for 40 μM, 400 μM and 1 mM concentration of (A) Ibuprofen and (B) Diclofenac in contacting solution.

It is evident, comparing the absolute resistance values from fitting across two substrates (Table S6, SI), that the initial resistance values vary from substrate to substrate. This is unsurprising, given the nature of the substrates, and is attributed to variations in the uniformity of cavity packing and consequent microscale roughness of gold substrate and surface coverage. Therefore, we compared data across several substrates and report the average relative changes in bilayer resistance and capacitance rather than absolute values as shown in Table 2. Ibu induces a modest but significant (by comparison with control, of a DOPC MSLB in absence of Ibu, Table S8, SI) and systematic decrease in bilayer resistance with increasing drug concentration. These changes were accompanied by small increases to the bilayer capacitance at higher drug concentrations. Together, the data indicate that the bilayer becomes more

permeable on Ibu interaction, which is attributed, from the modest change in capacitance, to decrease in membrane thickness indicating Ibu adsorption at the bilayer interface.

FLCS data indicated that compared to Ibu, Dic elicits very significant changes in the DOPC lipid membrane fluidity affecting both probes oriented at the aqueous membrane interface and within the hydrophobic core. Figure 4B shows the impedance response at a gold supported DOPC MSLB at different concentrations of Dic (0, 40, 400 and 1000μM). From visual inspection of the EIS response shown in Figure 4B, it is evident, and consistent with the FLCS data that Dic interacts in a more intimate way with the bilayer than Ibu. In contrast to Ibu, impedance decreases with increasing concentration of Dic at the DOPC membrane. Furthermore, the magnitudes of the relative change in impedance are significantly greater and evident even at the lowest concentration of Dic (1 μM). Removal of Dic from the contacting solution at the end of the titration left the impedance spectra relatively unchanged. This observation is consistent with FLCS data indicating the drug associates strongly, penetrates deeply and irreversibly into the phosphatidylcholine membrane.[5]

The resistance and capacitance data for Dic are summarized in Table 2. The data shown were collected from three independently prepared and studied gold cavity array substrates. As a control, the stability of bilayer at an intermediate Dic concentration of 100 μM was monitored and it was observed that no significant changes to the bilayer resistivity over 3-4 hrs (Fig. S2 and Table S7, SI). As Dic was prepared in a minimum volume of methanol to aid solubility, a control was conducted to ensure that the membrane resistance change was not due to membrane disruption by methanol (Figures S3, S4 and Table S9, SI). The impact of methanol at the concentration of 0.1% V/V used here, was insignificant compared with the impact of Dic, confirming that the change in resistance is due to Dic.

EIS shows that both Ibu and Dic induce systematic decreases in membrane resistance with increasing drug concentration. Consistent with FCS data, the magnitude of resistance change is far greater for Dic than Ibu indicating the former is impacting the lateral packing density of the membrane and significantly increasing its ion permeability. We did not observe a significant difference between the capacitance changes of the bilayer between Ibu and Dic, suggesting that the layer thickness in each case is comparable and only modestly affected by these drugs (Table 2).

Table 2: Effect of Ibu and Dic on the resistance and capacitance of DOPC bilayer at increasing concentrations. Results depict change (Δ) recorded following drug addition, relative to bilayer prior to drug interaction.

Concentration (μM)	Ibuprofen		Diclofenac	
	ΔRm (MΩcm²)	**ΔCm (μFcm⁻²)**	**ΔRm (MΩcm²)**	**ΔCm (μFcm⁻²)**
DOPC	0.00	0.00	0.00	0.00
1	-0.07 ± 0.06	0.00	0.98 ± 0.07	0.00
5	-0.30 ± 0.04	0.02 ± 0.02	-1.35 ± 0.13	0.03 ± 0.01
20	-0.39 ± 0.17	0.04 ± 0.03	-1.75 ± 0.20	0.05 ± 0.02
40	-0.51 ± 0.25	0.07 ± 0.04	-2.08 ± 0.32	0.05 ± 0.05
100	-0.72 ± 0.31	0.14 ± 0.03	-2.55 ± 0.50	0.18 ± 0.09
400	-0.72 ± 0.39	0.18 ± 0.05	-3.68 ± 0.56	0.25 ± 0.04
1000	-0.76 ± 0.46	0.25 ± 0.03	-3.64 ± 0.49	0.24 ± 0.08

Antibiotics: Rifampicin, Levofloxacin and Pefloxacin.

We examined three antibiotics, Rifampicin, and two synthetic fluoroquinolone antibiotics Levofloxacin and Pefloxacin. The impact of Rif on the fluidity of a DOPC lipid membrane was examined by varying the concentration of Rif from 1 - 20 μM. The experiments were performed, as described for Ibu and Dic and representative ACF curves are provided in the supplementary information (Figure S5A, SI). The data were fitted to a 2D-diffusion model and results are summarized in Table 3a,b. A complication in interrogating the Rif is that has a visible absorbance between 400 – 600 nm (Figure S6, SI) and at concentrations in excess of 20 μM, this feature masks the fluorescence signal from the probe resulting in rather noisy ACF data and very low molecular brightness for lipid probes.

With increasing concentration of Rif, *D* of ATTO increased dramatically to 209.5 ± 34.3 $\mu m^2 s^{-1}$ for 20 μM of drug (Table 3a). The α value for ATTO was also influenced by Rif and increased to 1.13 ± 0.14 at this concentration. The fluorescence lifetime and molecular brightness of ATTO in DOPC lipid bilayer were reduced from 3.3 ± 0.02 ns to 2.99 ± 0.04 ns and 6300 ± 600 cpsm to 1000 ± 100 cpsm with increasing concentration of Rif in the contacting solution. At the end of the titration, the membrane contacting buffer was exchanged for fresh PBS buffer to remove the drugs from the solution. Following this treatment, *D* of ATTO was 20.8 ± 5.2 $\mu m^2 s^{-1}$ and did not fully recover suggesting the Rif irreversibly associates/permeates with the membrane. Rif impacted the fluorescence correlation data for the DOPC membrane in an analogous way to Dic but the concentration of 20 μM at which the effect was observed was much lower for Rif.

To examine the impact of Rif on BODIPY diffusion, we studied 0.01, 0.1, 1 and 5 μM of Rif concentrations. At concentrations exceeding 5 μM, no ACF data were obtained and molecular brightness was very low due to the strong absorbance of Rif drug (data not shown). Table 3b shows diffusion data for BODIPY in DOPC membrane as a function of concentration of Rif. On increasing the concentration of the drug, D decreased to 6.38 ± 1.5 $\mu m^2 s^{-1}$ and α was reduced to 0.83 ± 0.04 for 5 μM. Similarly, the lifetime and molecular brightness of the BODIPY label within the bilayer decreased to 4.82 ± 0.18 ns and 4500 ± 1004 cpsm for 5 μM. The alteration to diffusion coefficient and probe lifetime indicates the drug impacts the probe environment which can only occur if Rif is penetrating into the hydrophobic core. However, measured molecular brightness changes may be due to the filtering of the excitation signal by Rif. On replacing the drug solution with fresh buffer in the microfluidic chamber the D, τ_i and MB values of the probe in the membrane are only partly recovered indicating Rif partitions strongly into the hydrophobic core of the membrane and is permeating the membrane (Table 3b).

Analogous FCS studies of Levo and Pef, in contact with DOPC MSLB, were carried out and the data are shown in Tables S10A and B (SI). The concentrations used in this study correspond to the reported plasma level which is in the range of 10 μM[54]. Notably, unlike Rif, neither Levofloxacin nor Pefloxacin exerted any significant impact on the D value of ATTO in DOPC membrane (Figure S7, SI). Similarly, the mobility of BODIPY probes in DOPC lipid membrane was not affected by the presence of 20 μM Levo and Pef in contacting solution (Table S11 SI), τ_i, MB, and α values for both probes also were unaffected by the presence of Levo and Pef.

Table 3: FLCS data analysis of ATTO and BODIPY in microcavity supported DOPC lipid bilayer as a function of Rif concentration

a) ATTO

Conc. (μM)	Mol. Brightness (X 1000) cpsm	Fluor. lifetime (ns)	Anomalous exponent α	D ($\mu m^2 s^{-1}$)
0	6.20 ± 0.9	3.30 ± 0.03	0.98 ± 0.03	11.71 ± 0.82
1	4.20 ± 0.3	3.21 ± 0.05	1.06 ± 0.09	19.58 ± 2.09
5	5.3 ± 0.3	3.27 ± 0.01	0.95 ± 0.03	48.83 ± 2.80
10	2.5 ± 0.3	3.10 ± 0.04	1.16 ± 0.08	125.7 ± 18.3
20	2.0 ± 0.2	2.99 ± 0.04	1.13 ± 0.14	209.5 ± 34.3
After wash	4.15 ± 0.9	3.10 ± 0.05	0.75 ± 0.12	20.8 ± 5.2

b) β-BODIPY-C_5-HPC

Conc. (μM)	Mol. Brightness (X 1000) cpsm	Fluor. lifetime (ns)	Anomalous exponent α	D ($\mu m^2 s^{-1}$)
0	12.45 ± 2.40	6.0 ± 0.1	0.95 ± 0.03	11.52 ± 1.20
0.01	12.81 ± 2.75	6.03 ± 0.09	0.97 ± 0.02	11.23 ± 0.74
0.1	10.20 ± 2.00	5.77 ± 0.26	0.93 ± 0.02	9.31 ± 0.56
1	6.50 ± 1.75	5.25 ± 0.16	0.82 ± 0.05	6.97 ± 1.14
5	4.50 ± 1.04	4.82 ± 0.14	0.83 ± 0.04	6.38 ± 1.50
After wash	9.58 ± 2.45	5.87 ± 0.13	0.93 ± 0.05	9.76 ± 1.23

Representative Nyquist plots for Rif (Fig. S8, SI), Levo and Pef (Figs. S9A and B) drugs on interaction with DOPC membrane at gold microcavity SLB are provided in supplementary information. The membrane resistance was observed to decrease with increasing drug concentration, across all of the antibiotics, but consistent with FCS, the effect was most pronounced for Rif and moderate for Levo and Pef. (Table 4). Similarly, the capacitance was increased in the presence of Rif, modestly increased for Levo and Pef did not measurably affect membrane capacitance (cf. Table 4). Given the inverse relationship between capacitance and the thickness of the dielectric, this response indicates the membrane becomes thinner in the presence of Rif. The direction and magnitude of the changes in the resistance data correlated well with changes in the diffusion coefficient observed for each drug.

Table 4: Effect of Rif, Levo and Pef on the resistance and capacitance of a DOPC lipid bilayer with increasing concentration. Results presented depict the change (Δ) recorded following drug addition, relative to bilayer prior to drug interaction.

[Drug] (μM)	Rifampicin		Levofloxacin		Pefloxacin	
	ΔRm ($M\Omega cm^2$)	**ΔCm ($\mu F cm^{-2}$)**	**ΔRm ($M\Omega cm^2$)**	**ΔCm ($\mu F cm^{-2}$)**	**ΔRm ($M\Omega cm^2$)**	**ΔCm ($\mu F cm^{-2}$)**
0	0	0	0	0	0	0
1	-0.21±0.02	0.05±0.001	-0.01±0.03	0.15±0.01	-0.06±0.02	0.08±0.001
5	-1.74±0.04	0.27±0.004	-0.11±0.02	0.23±0.01	-0.07±0.04	0.09±0.004
10	-4.119±0.03	0.47±0.08	-0.14±0.01	0.34±0.02	-0.082±0.03	-0.10±0.007
20	-4.365±0.02	0.97±0.01	-0.21±0.01	0.40±0.01	-0.12±0.01	-0.12±0.06

Interaction of Rifampicin with different lipid compositions

Given the evidence for permeation of the Rifampicin into the bilayer, we studied the interaction of Rif with different lipid compositions representative of bacterial membranes. Here, we used lipid mixtures

made from phosphatidylglycerol (PG), phosphatidylethanolamine (PE) and phosphatidylserine (PS). (PG and PE are the most prevalent lipids in bacterial membrane[55–57] and PS is anionic lipid from the mammalian membrane[55]) so that we could compare the impact of the anionic charge on the lipid, for PS and PG on drug interactions. These experiments were carried out as described for Rif interaction with DOPC lipid membrane, varying the concentration of Rif from 1 - 20 μM. Representative ACF data and analysis are provided as supplementary information (Figure S5 and Tables S12-S14, SI).

We examined Rif interaction at MSLBs with 3 different lipid compositions: DOPC:DOPG (4:1), DOPC:DOPS (4:1) and DOPC:DOPG:DOPE (3:1:1) (mole ratio). The *D* value of ATTO in all lipid mixtures increased with increasing concentration of drug, consistent with the data observed for pristine DOPC bilayer. However, by 20 μM Rif addition, *D* was found to be 52.60 ± 6.8 $\mu m^2 s^{-1}$ (Tables S12-S14, SI), which was approximately 4 times less than observed at the DOPC only bilayer. Figure 5 describes the relative change in lipid diffusion for a given concentration of Rif against the lipid diffusion without drugs for lipid mixtures. The impact of Rif was similar across all lipid compositions with no significant variation between DOPG and DOPS. The α value for ATTO in all the lipid mixtures was greater than 1 at 20 μM like behavior in a DOPC bilayer. Similarly, the fluorescence lifetime and molecular brightness of ATTO in DOPC:DOPG, DOPC:DOPS, DOPC:DOPG:DOPE was reduced on increasing the concentration of Rif, indicating the drug is disrupting the interfacial region of the bilayer, however the effect is dramatically reduced in the presence of anionic phospholipid. On conclusion of the titration, the membrane contacting buffer was exchanged for fresh PBS buffer and *D* value of ATTO was close to that found on exposure to 1 μM Rif indicating some Rif remains associated with the membrane (Tables S12-S14, SI).

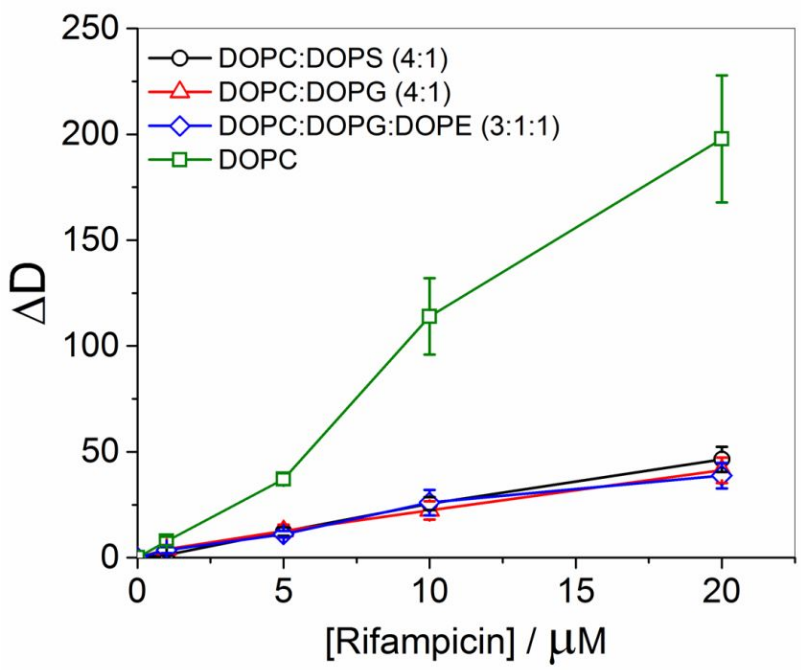

Figure 5: Change in diffusion coefficient ($\Delta D = D\text{-}D_0$) of Rifampicin in designated lipid mixtures: DOPC: DOPS [4:1] (○, black), DOPC: DOPG [4:1] (Δ, red), DOPC:DOPG:DOPE [3:1:1] (◊, blue), DOPC (□, olive). The *D* value was measured as a function of concentration of drug on lipid the composition described above using FLCS and bilayer was spread across the microcavity supported lipid bilayer.

Analogous EIS experiments were then completed to evaluate changes to membrane thickness and permeability. The changes in the resistance and capacitance for all the lipid compositions in the presence of Rif are summarized in Table 5. For all lipid compositions, membrane resistance decreased with increasing concentration of Rif (Fig. S10, SI). However consistent with the FLCS data, the magnitude of the resistance decrease is 4 times lower compared the DOPC-only membrane (Table 3). Notably, the magnitude of the decrease in bilayer resistance is far greater in the presence of DOPG compared to DOPS lipids. For example, at the highest concentration of Rif explored, 20 μM, the resistance had decreased on average by 1.63 MΩcm^2 for a DOPC:DOPS(4:1) MSLB composition compared to 2.49 MΩcm^2 and 4.65 MΩcm^2 for DOPC:DOPG(4:1) and DOPC:DOPG:DOPE(3:1:1) respectively. This indicates that although both DOPG and DOPS are acidic lipids (anionic at neutral pH) Rif interacts significantly more strongly with DOPG. Although by far the strongest perturbation of the bilayer is evident for the neutral DOPC-only bilayer. Clearly charge influences Rif interaction with the membrane, Rif is a neutral species at

physiological pH, it is zwitterionic and is both a H-bond donor and acceptor and such interactions likely inhibit penetration of the drug into charged bilayers.

Table 5: Resistance data for different lipid mixtures as a function of concentration of Rif. Results presented reflect the change (Δ) recorded following drug addition, relative to bilayer prior to drug interaction.

[Rif] (μM)	DOPC:DOPG(4:1)		DOPC:DOPS(4:1)		DOPC:DOPG:DOPE(3:1:1)	
	ΔRm ($M\Omega cm^2$)	**ΔCm (μFcm^{-2})**	**ΔRm ($M\Omega cm^2$)**	**ΔCm (μFcm^{-2})**	**ΔRm ($M\Omega cm^2$)**	**ΔCm (μFcm^{-2})**
0	0.00	0.00	0.00	0.00	0.00	0.00
1	-0.65 ± 0.08	-0.02± 0.03	-0.29 ± 0.05	0.01± 0.005	-1.88 ± 0.09	-0.03± 0.01
5	-1.09 ± 0.06	-0.02± 0.01	-0.77 ± 0.14	0.04± 0.02	-2.67 ± 0.41	0.00± 0.02
10	-1.83 ± 0.20	-0.09± 0.01	-1.34 ± 0.09	0.05± 0.03	-3.92 ± 0.35	0.02 ± 0.03
20	-2.49 ± 0.47	-0.13± 0.05	-1.63 ± 0.16	0.03± 0.01	-4.65 ± 0.23	0.03± 0.03

Notably, in the presence of anionic lipid, the impact of Rif on membrane capacitance is negligible when compared with DOPC only bilayer. It is also interesting to note that among the three mixed bilayer compositions, the magnitude of change in capacitance is greater for DOPC:DOPG bilayer than DOPC:DOPS and DOPC:DOPG:DOPE bilayers.

Bisphosphonates: Alendronate and Clodronate

Finally, we studied the interaction of membrane impermeable bisphosphonate drugs, Alendronate and Clodronate with the DOPC membrane. Bisphosphonates are acidic and thus we carried out the study at pH 5.25. The Langmuir-Blodgett trough and microcavities were filled with Tris buffer, pH 5.25, 137 mM NaCl, and DOPC lipids were transferred from subphase to form monolayers above the cavities. The DOPC vesicles were prepared using the same buffer and allowed to disrupt above the lipid monolayer to form a bilayer. Otherwise, the experimental setup and procedure were identical to those above. The drugs

were dissolved in the Tris buffer and pH was adjusted to match that of the whole system (pH 5.25). From FCS, the *D* value of ATTO in DOPC lipid membrane was 11.00 ± 0.8 $\mu m^2 s^{-1}$ for Tris buffer, pH 5.25, and as expected is consistent with the value calculated in contact with PBS buffer, pH 7.4. The concentration of drug was increased from 1 to 4 mM in 1 mM step and the *D* value of ATTO probe was measured at each concentration. Neither Alen nor Clo, induced a change in the *D*, α, *τ* and MB in DOPC lipid membrane (Table S15, SI). Furthermore, we studied BODIPY in DOPC lipid membrane at a drug concentration of 4 mM and for both the drugs (Table S16, SI), again no notable changes were observed for *D*, *α*, *τ* and MB indicating the absence of any permeation of drugs across the lipid bilayer.

The interaction of bisphosphonate with a DOPC membrane in Tris buffer, pH 5.25 was studied using EIS. The stability of the bilayer at this pH was first examined by EIS (Figure S11, SI). The constant impedance indicated the DOPC bilayer was stable over the 5 hour window required for the measurement. Then, we systematically introduce the bisphosphonate drugs into the contacting medium and measured EIS as described above. In the case of Alen, no significant changes were observed in membrane resistance, but the small reduction in the capacitance suggested some adsorption of Alen on the DOPC membrane surface. The resistance and capacitance values remain invariable upon interaction with Clo over the concentration range of 1-4 mM (Table 6).

Table 6: Resistance and capacitance changes as a function of the concentration of Alen and Clo. Results reflect the change (Δ) following drug addition, relative to bilayer prior to drug interaction.

[Drug] (mM)	Alendronates		Clodronates	
	ΔRm ($M\Omega cm^2$)	**ΔCm ($\mu F cm^{-2}$)**	**ΔRm ($M\Omega cm^2$)**	**ΔCm ($\mu F cm^{-2}$)**
0	0	0	0	0
1	-0.24 ± 0.05	-0.75 ± 0.4	0.13 ± 0.8	-0.02± 0.01
2	-0.05 ± 0.05	2.0 ± 0.5	0.19 ± 0.4	0.02 ± 0.02
4	-0.25 ± 0.15	2.01 ± 0.7	0.29 ± 0.15	0.03 ± 0.02

Discussion

There are two mechanisms that have been ascribed to molecular permeation across a pure lipid membrane; the solubility-diffusion (SD) and the transient-pore (TP) mechanisms[58]. In SD, the drug is said to partition into the lipid membrane, diffuse through the core and then partition into solution. In the TP mechanism, transient pores instigated by thermal fluctuations of the membrane are thought to promote permeation[59]. In both cases, the adsorption of the drug at the membrane interface precedes permeation.

EIS is expected to be sensitive to these processes, where porosity is increasing, resistance decreases and capacitance can increase due to thinning of the bilayer. Where adsorption is occurring without permeation, the capacitance may increase without accompanying changes to membrane resistance or fluidity.

From EIS data it is clear that the bilayer resistance (ΔR) increases with drug concentration reaches saturation (Tables 2 and 4); the resulting curves as shown in Figure 6, can be fitted using Langmuir-Freundlich (LF) model.

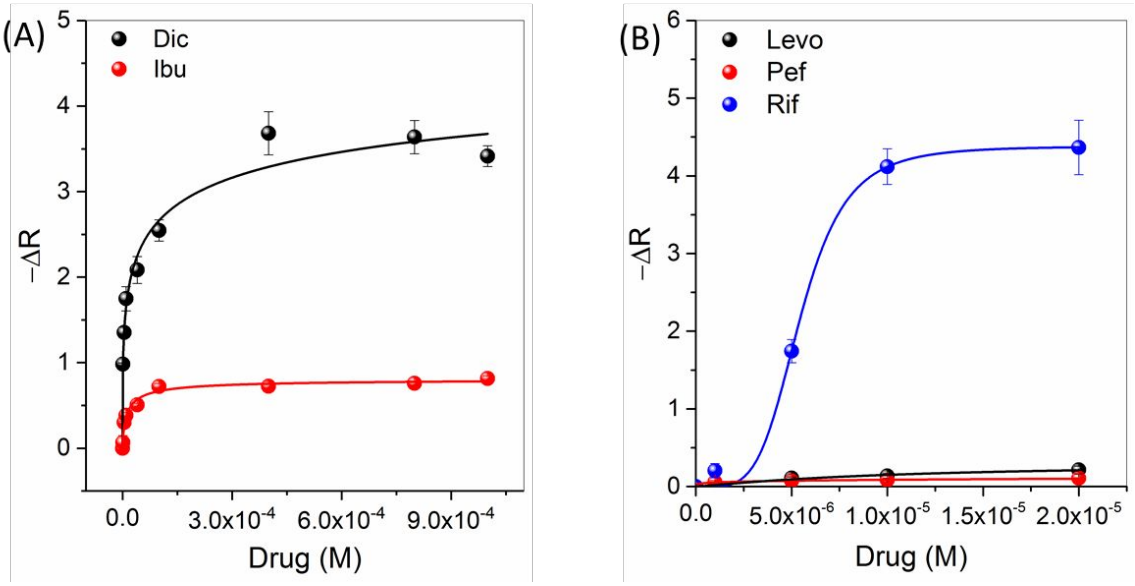

Figure 6: EIS data fitted to non-linear Langmuir-Freundlich (solid line) Isotherms for different drugs, A: Dic and Ibu, and B: Levo, Pef and Rif using Eqn. (4). ΔR correspond the change in membrane resistance after drug addition compared to membrane alone.

Like EIS studies, the relative change in lipid diffusion coefficient of ATTO probe as a function of drug concentration for both Ibu and Dic at the MSLB (Figure S12, SI) also exhibited a sigmoidal response, suggesting saturation binding. However, the modest impact of Ibu on membrane fluidity meant that a reliable binding curve could not be obtained from FLCS data for this drug. Nonetheless, from the EIS data shown in Figure 6A, the plateau regions (saturation binding) occur at approximately 400 μM for Dic and 100 μM for Ibu. Such a dependence of drug concentration on the physical characteristics of the membrane could be attributed to membrane binding and thus Langmuir-Freundlich isotherm was used to describe the adsorption of the drug onto the DOPC MSLB. On this basis, R_{sat} and a binding constant, K_a

were estimated by non-linear regression analysis and values are summarized in Table 7 along with the reported clogP and P_{app} values for each drug[60].

From the data shown in Fig. 6A and B, we observed good fit ($R^2 > 0.97$, cf. Table 7) to LF isotherms for all of the drugs explored. The calculated values, of course, are not absolute and will depend on experimental conditions such as membrane area. Nonetheless, for drugs at a given bilayer platform these parameters are a useful empirical measure of the impact of each drug on the lipid bilayer. With the exception of Ibuprofen the R_{sat} values correlate reasonably well with both Papp and cLogP. K_a values conversely do not correlate with these parameters. For example, Rsat is similar for Ibu and Rif and they are the two most lipophilic of the drugs investigated. Nonethless K_a calculated from the fits as 1.82 $x10^5$ M^{-1} for Rif compared with 0.09 $x10^5$ M^{-1} for Dic. Because the drugs are not merely adsorbing at the membrane the low K_a value for Dic from the LF model is tentatively attributed to the high penetration into and passive permeation of this drug across the membrane whereas Rif may be retained more strongly at the membrane.

Table 7: Association constants calculated for drugs by fitting relative change in DOPC membrane to non-linear Langmuir-Freundlich isotherm model. The clogP and P_{app} parameters are literature reported values.

Drug	clogP[61]	K_a ($x10^5$)	R_{sat}	n	R^2	P_{app} (x 10^{-6} cm/sec)[a]
Ibuprofen	3.679	0.78±0.18	0.81±0.02	0.74	0.97	10.1 ± 0.2[62]
Diclofenac	4.726	0.09±0.1	5.42±1.9	0.33	0.97	13.28 ± 0.2[63]
Rifampicin	2.77	1.82±0.08	4.38±0.15	4.55	0.99	5.0 ± 0.20[64]
Levofloxicin	-0.879	0.95±0.2	0.31±0.08	1.1	0.96	0.26 ± 0.005~[65]
Pefloxicin	0.27	5.32±.3	0.09±0.01	1.2	0.99	
Alendronate	-5.642	--	--			
Clodronate	-2.40	--	--			0.05 ± 0.002[66]

[a]apparent permeability coefficient of drugs in Caco-2 cells; ~ Egg-Phosphatidylcholine lipids

EIS and FLCS data indicate Ibu interaction with the DOPC bilayer at pH 7.4 is confined to weak interactions at the interface of the bilayer which do not affect lipid lateral mobility. Several studies on interaction Ibu with phosphocholine bilayers show the fluidity of the membrane was unaltered leading to the conclusion that the drug resides close to the head group through non-covalent interaction with lipids.[5,67–69,69] Consistent with this picture, our data suggest surface binding of the ibuprofen to the bilayer,

most likely through electrostatic interaction between the quaternary ammonium part of choline head group and the anionic Ibu. This finding contrasts with *in vivo* studies on cell lines which clearly show Ibu transports across the cell membrane. The P_{app} values of ibuprofen in different cell lines including Caco-2 cells are > 10 x 10^{-6} cm/s consistent with high absorption/permeability across the membrane.[62,63,70]. Interestingly, Novakova et. al, found the transport of Ibu was reduced significantly in the absence of serum and Ibu strongly binds to serum.[70] Overall, the strong consistency of evidence across model studies and the contrast between biophysical model and cells is consistent with active transport of Ibu within cells mediated by plasma or extracellular proteins and that passive transport is likely to be weak.

In the case of Dic, numerous biophysical studies have demonstrated that this compound exerts a strong interaction with the membrane core. [31,71,72] From our data, the decrease in fluorescence lifetime and increase in diffusion coefficient suggests that the ATTO probe itself interacts strongly with the Dic bound at the interface, possibly lifting the probe from the membrane

However, τ_i and MB of the BODIPY probe decreased which is strongly suggestive of drug permeation through the membrane. The lateral mobility of the hydrophobic probe was reduced in the presence of Dic, indicating a change in the fluidity of the membrane, whilst the anomalous exponent was unchanged, indicating normal diffusion.

The calculated K_a value for Dic is low compared to Ibu (Table 7) and reported P_{app} for Dic in different cell lines is > 10 x 10^{-6} cm/s suggesting that the drug strongly adsorbs and permeates across the membrane. Overall, our results, combined with reported cell uptake data suggest that whereas Ibu is likely primarily transported through membranes via an active mechanism, Dic is likely to be strongly passively transported across cell membranes. Importantly, membrane capacitance changes were positive and of similar magnitude for both drugs indicating a modest decrease in membrane thickness. However, in each case the membrane integrity is preserved on drug binding, consistent with low membrane toxicity.

Similarly, Langmuir-Freundlich isotherm applied to membrane resistivity for Rif yielded an excellent fit with a $R^2 > 0.99$. The "n" constant in the LF model (Eq. 4) relates to the strength of the adsorption. The n <1 observed here indicates chemically mediated absorption, n =1 suggests a linear relationship between the quantity absorbed and the equilibrium drug concentration and n > 1 indicates slightly unfavorable absorption. In our case, n = 4.33 (Table 7) suggesting a highly unfavorable process due to competition with water for absorption sites or more likely due to permeation across the membrane[73]. In agreement with EIS, our FLCS studies, revealed fast diffusion of DOPE labeled with an ATTO probe, along with a significant reduction in the fluorescence lifetime and molecular brightness indicating the association of Rif with the headgroup of the bilayer. In contrast to ATTO, the BODIPY probe, which is located in the

hydrophobic core of the bilayer, exhibits reduced diffusion for Rif concentrations exceeding 5 μM with accompanying reductions in τ_T and MB. This indicates that Rif permeates the core, passively diffusing across the bilayer. Our results are consistent with a previous study by Rodrigues et al. based on fluorescence quenching of probes located at the surface and an inner core of a DPPC bilayer[74]. The similar quenching efficiency for both probes suggested Rif permeates the membrane core.[75]

Both FLCS and EIS data reflect similar differences between Rif and DOPC-only membrane and membranes containing negatively charged lipids. From EIS data the change in membrane resistivity was plotted against Rif concentration for various lipid compositions and data were fitted to the Langmuir-Freundlich model (Figure 6B and Figure S13, SI) to give a calculated association constant K_a = 1.8 x 10^5 M^{-1} for DOPC lipids (Table 7) and 0.19 x 10^5 M^{-1} for a membrane containing DOPG lipids (Table S17, SI). The distinction is comparable to partition coefficients (K_p) determined for Rif with DMPC liposomes (5.09 x 10^4) and DOPG liposomes (0.54 x 10^4).[74] Recent isothermal titration calorimetry studies on POPC and ternary lipid mixtures POPE/POPC/POPG gave K_p = 1.9 x 10^3 for POPC and 8 x 10^1 for a ternary lipids membrane in the presence of Rif.[56] These data clearly indicate that Rif interacts specifically with PC and PG lipids. Consistent with this report, we obtained a different association constant for Rif in these lipid compositions (Table 7 and Table S17, SI). For DOPE:DOPG:DOPC, K_a was obtained as 0.77 x 10^5 M^{-1} which is lower than DOPC aloneand consistent with data reported for liposomes.[56] As Rif is zwitterionic at physiological pH (7.4) with 40% in the anionic form. The lower affinity of Rif for DOPC:DOPG:DOPE (representative of a bacterial membrane) maybe attributed in part to repulsion between the ionized Rif and negatively charged lipids. In addition, high lateral packing of the membrane due to the presence of phosphatidylethanolamine and phosphatidylglycerol /phosphatidylserine may also reduce the permeability of the drug in such membranes. In particular, lipid-lipid spacing decreases in the presence of PE lipids, due to additional hydrogen bonds with neighboring molecules through the amine headgroup.[76,77]

For Rif at a DOPS enriched lipid membrane, the lateral mobility of ATTO was the same as for DOPG enriched membranes. However, the relative change in membrane resistivity was different, as detected by the EIS technique which is more sensitive to changes in membrane structure than FCS. The relative change was -1.63 ± 0.16 $M\Omega cm^2$ for the DOPS membrane compared to -2.49 ± 0.47 $M\Omega cm^2$ for the DOPG membrane and both can be fitted to the LF model with R^2 = 0.99. The significant difference in the affinity of Rif with the charged lipids cannot be explained solely by charge repulsion.

In contrast to Rif, change in the membrane resistivity for Levo can be fitted to a Langmuir Isotherm with $R^2 > 0.99$ suggesting that this drug adsorbs onto the DOPC membrane interface. Although we observed a moderate increase in the membrane capacitance, the lateral mobility of ATTO and BODIPY in the DOPC membrane was relatively unchanged. Conversely, for Pef, we did not observe a significant change in resistivity or capacitance. Langmuir isotherm fit yielded $R^2 > 0.90$ indicating minimal absorption on the membrane. Similarly, diffusivity of ATTO and BODIPY was relatively unchanged. The reported P_{app} value for Levo in Caco-2 cells is $< 1 \times 10^{-6}$ cm/s which is considered poor absorption. It has been proposed that these drugs are transported in membranes through an active mechanism by transporter proteins[78–80] rather than by passive diffusion, which is consistent with our study.

Finally, the bisphosphonate drugs studied on DOPC MSLBs had a very little impact on the fluorescence or electrochemical properties of the films. The diffusivity of ATTO and BODIPY probes in a DOPC membrane was unaltered in the presence of the drugs. Similarly, no change in the membrane resistivity was observed for Alendronate and only a slight increase was observed for Clodronate at a concentration of 4mM. Conversely, an increase in membrane capacitance was observed with Alen for concentrations ≥2 mM which may suggest that the film thickness has decreased. This is tentatively attributed to adsorption of the drugs at the membrane interface, at higher concentrations. The low P_{app} and high hydrophilicity indicate that these drugs are poorly permeable to the membrane and they are believed to be transported across the membrane through a paracellular route[66,81]. Our data support these conclusions.

Conclusions: Using FLCS and EIS along with microcavity supported lipid bilayer membranes we compare for the first time the impact that commonly administered anti-inflammatory, antibiotic and bisphosphonate drugs have on lipid membrane fluidity and electrochemical properties.

Upon systematically varying the concentration of drugs over therapeutic ranges, we measure the lipid membrane diffusion coefficient along with the fluorescence lifetime (τ_i) and molecular brightness (MB) of the lipid probe using FLCS. In parallel, we investigated the changes in membrane resistivity and capacitance using EIS.

Neither the mobility of the lipid probes nor their photophysical properties were altered on exposure of bilayer to Ibu, Levo or Pef. However, a modest decrease in the membrane resistivity was observed for each, indicating these drugs adsorb primarily at the membrane-aqueous interface with relatively weak penetration into the bilayer. The quenching of BODIPY fluorescence signal indicated that Dic and Rif pass through the membrane whilst membrane resistivity decreases very significantly in the presence of Dic indicating ion leakiness/porosity of the membrane is increased on binding by Dic and Rif. In the case

of the ATTO probe, faster mobility and α above 1 suggested that the membrane surface was partially disrupted, plausibly by direct interactions of the probe with Dic at the interface.

Overall, our data suggest that Dic and Rif interact with the lipid head groups, perturbing the membrane packing and permeating across the membrane, whereas other drugs more likely reside on the membrane-water interface. Our data are consistent with previous reports that Ibu, Levo and Pef are poorly passively permeable at a lipid bilayer whereas Dic and Rif display significant passive permeation. The relative changes in membrane resistivity can be fitted to a Langmuir-Freundlich Isotherms which provides empirical quantitative insight into the relative strength of the interaction of each drug with the membrane.

The interaction of Rif with the membrane was strongly dependent on the lipid composition; for binary and ternary mixtures of DOPC:DOPG:DOPS, the lateral mobility of ATTO was 4 times less than for DOPC lipid alone for Rif permeation. In the case of Alen and Clo no changes to lipid mobility or membrane resistivity were observed up to very high concentrations. These drugs are strongly hydrophilic and believed to permeate through a paracellular pathway, which requires minimal or no interaction with the lipid membrane.

Overall, the reported data are consistent with literature mechanisms proposed for drug-membrane interactions suggesting that MSLB models are a useful platform to study the interaction of drugs with the physiological membrane.

Acknowledgments: This material is based upon work supported by the Science Foundation Ireland under Grant No. [14/IA/2488]. T.E.K. and S.R are grateful to the Irish Research Council, Government of Ireland for the financial support via postdoctoral fellowships (GOIPD/2014/322). S.R is grateful to Science Foundation Ireland for the financial support for SFI Industrial fellowship.

References

(1) Peetla, C.; Stine, A.; Labhasetwar, V. Biophysical Interactions with Model Lipid Membranes: Applications in Drug Discovery and Drug Delivery. *Mol. Pharm.* **2009**, *6* (5), 1264–1276. https://doi.org/10.1021/mp9000662.

(2) Seddon, A. M.; Casey, D.; Law, R. V.; Gee, A.; Templer, R. H.; Ces, O. Drug Interactions with Lipid Membranes. *Chem. Soc. Rev.* **2009**, *38* (9), 2509–2519. https://doi.org/10.1039/B813853M.

(3) Lichtenberger, L. M.; Wang, Z.-M.; Romero, J. J.; Ulloa, C.; Perez, J. C.; Giraud, M.-N.; Barreto, J. C. Non-Steroidal Anti-Inflammatory Drugs (NSAIDs) Associate with Zwitterionic Phospholipids: Insight into the Mechanism and Reversal of NSAID-Induced Gastrointestinal Injury. *Nat. Med.* **1995**, *1* (2), 154–158. https://doi.org/10.1038/nm0295-154.

(4) Redondo-Morata, L.; Lea Sanford, R.; Andersen, O. S.; Scheuring, S. Effect of Statins on the Nanomechanical Properties of Supported Lipid Bilayers. *Biophys. J.* **2016**, *111* (2), 363–372. https://doi.org/10.1016/j.bpj.2016.06.016.

(5) Lichtenberger, L. M.; Zhou, Y.; Jayaraman, V.; Doyen, J. R.; O'Neil, R. G.; Dial, E. J.; Volk, D. E.; Gorenstein, D. G.; Boggara, M. B.; Krishnamoorti, R. Insight into NSAID-Induced Membrane Alterations, Pathogenesis and Therapeutics: Characterization of Interaction of NSAIDs with Phosphatidylcholine. *Biochim. Biophys. Acta BBA - Mol. Cell Biol. Lipids* **2012**, *1821* (7), 994–1002. https://doi.org/10.1016/j.bbalip.2012.04.002.

(6) Lacour, S.; Hammann, A.; Grazide, S.; Lagadic-Gossmann, D.; Athias, A.; Sergent, O.; Laurent, G.; Gambert, P.; Solary, E.; Dimanche-Boitrel, M.-T. Cisplatin-Induced CD95 Redistribution into Membrane Lipid Rafts of HT29 Human Colon Cancer Cells. *Cancer Res.* **2004**, *64* (10), 3593–3598. https://doi.org/10.1158/0008-5472.CAN-03-2787.

(7) Nunes, C.; Brezesinski, G.; Lopes, D.; Lima, J. L. F. C.; Reis, S.; Lúcio, M. Lipid-Drug Interaction: Biophysical Effects of Tolmetin on Membrane Mimetic Systems of Different Dimensionality. *J. Phys. Chem. B* **2011**, *115* (43), 12615–12623. https://doi.org/10.1021/jp206013z.

(8) Rebillard, A.; Tekpli, X.; Meurette, O.; Sergent, O.; LeMoigne-Muller, G.; Vernhet, L.; Gorria, M.; Chevanne, M.; Christmann, M.; Kaina, B.; et al. Cisplatin-Induced Apoptosis Involves Membrane Fluidification via Inhibition of NHE1 in Human Colon Cancer Cells. *Cancer Res.* **2007**, *67* (16), 7865–7874. https://doi.org/10.1158/0008-5472.CAN-07-0353.

(9) L. Armstrong, C.; Sandqvist, E.; C. Rheinstadter, M. Protein-Protein Interactions in Membranes. *Protein Pept. Lett.* **2011**, *18* (4), 344–353. https://doi.org/10.2174/092986611794653941.

(10) Darvas, M.; Hoang, P. N. M.; Picaud, S.; Sega, M.; Jedlovszky, P. Anesthetic Molecules Embedded in a Lipid Membrane: A Computer Simulation Study. *Phys. Chem. Chem. Phys.* **2012**, *14* (37), 12956–12969. https://doi.org/10.1039/C2CP41581J.

(11) Patrick, G. L. *An Introduction to Medicinal Chemistry*; OUP Oxford, 2013.

(12) Yamamoto, T.; Umegawa, Y.; Tsuchikawa, H.; Matsumori, N.; Hanashima, S.; Murata, M.; Haser, R.; Rawlings, B. J.; Caffrey, P. Role of Polyol Moiety of Amphotericin B in Ion Channel Formation and Sterol Selectivity in Bilayer Membrane. *Bioorg. Med. Chem.* **2015**, *23* (17), 5782–5788. https://doi.org/10.1016/j.bmc.2015.07.009.

(13) Kamiński, D. M.; Pociecha, D.; Górecka, E.; Gagoś, M. The Influence of Amphotericin B on the Molecular Organization and Structural Properties of DPPC Lipid Membranes Modified by Sterols. *J. Mol. Struct.* **2015**, *1082*, 7–11. https://doi.org/10.1016/j.molstruc.2014.10.081.

(14) Maher, S.; Basit, H.; Forster, R. J.; Keyes, T. E. Micron Dimensioned Cavity Array Supported Lipid Bilayers for the Electrochemical Investigation of Ionophore Activity. *Bioelectrochemistry* **2016**, *112*, 16–23. https://doi.org/10.1016/j.bioelechem.2016.07.002.

(15) Becucci, L.; Innocenti, M.; Salvietti, E.; Rindi, A.; Pasquini, I.; Vassalli, M.; Foresti, M. L.; Guidelli, R. Potassium Ion Transport by Gramicidin and Valinomycin across a Ag(1 1 1)-Supported Tethered Bilayer Lipid Membrane. *Electrochimica Acta* **2008**, *53* (22), 6372–6379. https://doi.org/10.1016/j.electacta.2008.04.043.

(16) Rose, L.; Jenkins, A. T. A. The Effect of the Ionophore Valinomycin on Biomimetic Solid Supported Lipid DPPTE/EPC Membranes. *Bioelectrochemistry* **2007**, *70* (2), 387–393. https://doi.org/10.1016/j.bioelechem.2006.05.009.

(17) Wenlock, M. C.; Austin, R. P.; Barton, P.; Davis, A. M.; Leeson, P. D. A Comparison of Physiochemical Property Profiles of Development and Marketed Oral Drugs. *J. Med. Chem.* **2003**, *46* (7), 1250–1256. https://doi.org/10.1021/jm021053p.

(18) Berquand, A.; Fa, N.; Dufrêne, Y. F.; Mingeot-Leclercq, M.-P. Interaction of the Macrolide Antibiotic Azithromycin with Lipid Bilayers: Effect on Membrane Organization, Fluidity, and Permeability. *Pharm. Res.* **2005**, *22* (3), 465–475. https://doi.org/10.1007/s11095-004-1885-8.

(19) Purushothaman, S.; Cama, J.; F. Keyser, U. Dependence of Norfloxacin Diffusion across Bilayers on Lipid Composition. *Soft Matter* **2016**, *12* (7), 2135–2144. https://doi.org/10.1039/C5SM02371H.
(20) Bourgaux, C.; Couvreur, P. Interactions of Anticancer Drugs with Biomembranes: What Can We Learn from Model Membranes? *J. Controlled Release* **2014**, *190*, 127–138. https://doi.org/10.1016/j.jconrel.2014.05.012.
(21) Khan, M. S.; Dosoky, N. S.; Williams, J. D. Engineering Lipid Bilayer Membranes for Protein Studies. *Int. J. Mol. Sci.* **2013**, *14* (11), 21561–21597. https://doi.org/10.3390/ijms141121561.
(22) Kiessling, V.; Domanska, M. K.; Murray, D.; Wan, C.; Tamm, L. K.; Begley, T. P. Supported Lipid Bilayers. In *Wiley Encyclopedia of Chemical Biology*; John Wiley & Sons, Inc., 2007.
(23) Basit, H.; Van der Heyden, A.; Gondran, C.; Nysten, B.; Dumy, P.; Labbé, P. Tethered Bilayer Lipid Membranes on Mixed Self-Assembled Monolayers of a Novel Anchoring Thiol: Impact of the Anchoring Thiol Density on Bilayer Formation. *Langmuir* **2011**, *27* (23), 14317–14328. https://doi.org/10.1021/la202847r.
(24) White, R. J.; Ervin, E. N.; Yang, T.; Chen, X.; Daniel, S.; Cremer, P. S.; White, H. S. Single Ion-Channel Recordings Using Glass Nanopore Membranes. *J. Am. Chem. Soc.* **2007**, *129* (38), 11766–11775. https://doi.org/10.1021/ja073174q.
(25) Meadows, K. E.; Nadappuram, B. P.; Unwin, P. R. A New Approach for the Fabrication of Microscale Lipid Bilayers at Glass Pipets: Application to Quantitative Passive Permeation Visualization. *Soft Matter* **2014**, *10* (42), 8433–8441. https://doi.org/10.1039/c3sm51406d.
(26) Lazzara, T. D.; Carnarius, C.; Kocun, M.; Janshoff, A.; Steinem, C. Separating Attoliter-Sized Compartments Using Fluid Pore-Spanning Lipid Bilayers. *ACS Nano* **2011**, *5* (9), 6935–6944. https://doi.org/10.1021/nn201266e.
(27) Basit, H.; Gaul, V.; Maher, S.; Forster, R. J.; Keyes, T. E. Aqueous-Filled Polymer Microcavity Arrays: Versatile & Stable Lipid Bilayer Platforms Offering High Lateral Mobility to Incorporated Membrane Proteins. *Analyst* **2015**, *140* (9), 3012–3018. https://doi.org/10.1039/C4AN02317J.
(28) Jose, B.; Mallon, C. T.; Forster, R. J.; Blackledge, C.; Keyes, T. E. Lipid Bilayer Assembly at a Gold Nanocavity Array. *Chem. Commun.* **2011**, *47* (46), 12530–12532. https://doi.org/10.1039/C1CC15709D.
(29) Böhmer, M.; Wahl, M.; Rahn, H.-J.; Erdmann, R.; Enderlein, J. Time-Resolved Fluorescence Correlation Spectroscopy. *Chem. Phys. Lett.* **2002**, *353* (5–6), 439–445. https://doi.org/10.1016/S0009-2614(02)00044-1.
(30) Benda, A.; Fagul'ová, V.; Deyneka, A.; Enderlein, J.; Hof, M. Fluorescence Lifetime Correlation Spectroscopy Combined with Lifetime Tuning: New Perspectives in Supported Phospholipid Bilayer Research. *Langmuir* **2006**, *22* (23), 9580–9585. https://doi.org/10.1021/la061573d.
(31) Basit, H.; Lopez, S. G.; Keyes, T. E. Fluorescence Correlation and Lifetime Correlation Spectroscopy Applied to the Study of Supported Lipid Bilayer Models of the Cell Membrane. *Methods* **2014**, *68* (2), 286–299. https://doi.org/10.1016/j.ymeth.2014.02.005.
(32) Dertinger, T.; Pacheco, V.; von der Hocht, I.; Hartmann, R.; Gregor, I.; Enderlein, J. Two-Focus Fluorescence Correlation Spectroscopy: A New Tool for Accurate and Absolute Diffusion Measurements. *ChemPhysChem* **2007**, *8* (3), 433–443. https://doi.org/10.1002/cphc.200600638.
(33) Haustein, E.; Schwille, P. Fluorescence Correlation Spectroscopy: Novel Variations of an Established Technique. *Annu. Rev. Biophys. Biomol. Struct.* **2007**, *36* (1), 151–169. https://doi.org/10.1146/annurev.biophys.36.040306.132612.
(34) Guigas, G.; Weiss, M. Sampling the Cell with Anomalous Diffusion—The Discovery of Slowness. *Biophys. J.* **2008**, *94* (1), 90–94. https://doi.org/10.1529/biophysj.107.117044.

(35) Kapusta, P.; Macháň, R.; Benda, A.; Hof, M. Fluorescence Lifetime Correlation Spectroscopy (FLCS): Concepts, Applications and Outlook. *Int. J. Mol. Sci.* **2012**, *13* (10), 12890–12910. https://doi.org/10.3390/ijms131012890.

(36) *Principles of Fluorescence Spectroscopy | Joseph R. Lakowicz | Springer*.

(37) Qian, H.; Elson, E. L. Distribution of Molecular Aggregation by Analysis of Fluctuation Moments. *Proc. Natl. Acad. Sci.* **1990**, *87* (14), 5479–5483. https://doi.org/10.1073/pnas.87.14.5479.

(38) Unruh, J. R.; Gratton, E. Analysis of Molecular Concentration and Brightness from Fluorescence Fluctuation Data with an Electron Multiplied CCD Camera. *Biophys. J.* **2008**, *95* (11), 5385–5398. https://doi.org/10.1529/biophysj.108.130310.

(39) Soares, J. C.; Soares, A. C.; Pereira, P. A. R.; Rodrigues, V. da C.; Shimizu, F. M.; Melendez, M. E.; Neto, C. S.; Carvalho, A. L.; Leite, F. L.; Machado, S. A. S.; et al. Adsorption According to the Langmuir–Freundlich Model Is the Detection Mechanism of the Antigen P53 for Early Diagnosis of Cancer. *Phys. Chem. Chem. Phys.* **2016**, *18* (12), 8412–8418. https://doi.org/10.1039/C5CP07121F.

(40) Ramadurai, S.; Holt, A.; Krasnikov, V.; van den Bogaart, G.; Killian, J. A.; Poolman, B. Lateral Diffusion of Membrane Proteins. *J. Am. Chem. Soc.* **2009**, *131* (35), 12650–12656. https://doi.org/10.1021/ja902853g.

(41) Gaul, V.; Lopez, S. G.; Lentz, B. R.; Moran, N.; Forster, R. J.; Keyes, T. E. The Lateral Diffusion and Fibrinogen Induced Clustering of Platelet Integrin AIIbβ3 Reconstituted into Physiologically Mimetic GUVs. *Integr. Biol.* **2015**, *7* (4), 402–411. https://doi.org/10.1039/C5IB00003C.

(42) Mehlisch, D. R.; Sykes, J. Ibuprofen Blood Plasma Levels and Onset of Analgesia. *Int. J. Clin. Pract.* **2013**, *67*, 3–8. https://doi.org/10.1111/ijcp.12053.

(43) Heyneman, C. A.; Lawless-Liday, C.; Wall, G. C. Oral versus Topical NSAIDs in Rheumatic Diseases. *Drugs* **2000**, *60* (3), 555–574. https://doi.org/10.2165/00003495-200060030-00004.

(44) Koenigsknecht, M. J.; Baker, J. R.; Wen, B.; Frances, A.; Zhang, H.; Yu, A.; Zhao, T.; Tsume, Y.; Pai, M. P.; Bleske, B. E.; et al. In Vivo Dissolution and Systemic Absorption of Immediate Release Ibuprofen in Human Gastrointestinal Tract under Fed and Fasted Conditions. *Mol. Pharm.* **2017**, *14* (12), 4295–4304. https://doi.org/10.1021/acs.molpharmaceut.7b00425.

(45) Karolin, J.; Johansson, L. B.-A.; Strandberg, L.; Ny, T. Fluorescence and Absorption Spectroscopic Properties of Dipyrrometheneboron Difluoride (BODIPY) Derivatives in Liquids, Lipid Membranes, and Proteins. *J. Am. Chem. Soc.* **1994**, *116* (17), 7801–7806. https://doi.org/10.1021/ja00096a042.

(46) Ariola, F. S.; Mudaliar, D. J.; Walvick, R. P.; Heikal, A. A. Dynamics Imaging of Lipid Phases and Lipid-Marker Interactions in Model Biomembranes. *Phys. Chem. Chem. Phys.* **2006**, *8* (39), 4517–4529. https://doi.org/10.1039/B608629B.

(47) Miyatake, S.; Ichiyama, H.; Kondo, E.; Yasuda, K. Randomized Clinical Comparisons of Diclofenac Concentration in the Soft Tissues and Blood Plasma between Topical and Oral Applications. *Br. J. Clin. Pharmacol.* **2009**, *67* (1), 125–129. https://doi.org/10.1111/j.1365-2125.2008.03333.x.

(48) Tabarin, T.; Martin, A.; Forster, R. J.; Keyes, T. E. Poly-Ethylene Glycol Induced Super-Diffusivity in Lipid Bilayer Membranes. *Soft Matter* **2012**, *8* (33), 8743–8751. https://doi.org/10.1039/C2SM25742D.

(49) Naumowicz, M.; Figaszewski, Z. A. Impedance Analysis of Lipid Domains in Phosphatidylcholine Bilayer Membranes Containing Ergosterol. *Biophys. J.* **2005**, *89* (5), 3174–3182. https://doi.org/10.1529/biophysj.105.063446.

(50) Nikolov, V.; Lin, J.; Merzlyakov, M.; Hristova, K.; Searson, P. C. Electrical Measurements of Bilayer Membranes Formed by Langmuir−Blodgett Deposition on Single-Crystal Silicon. *Langmuir* **2007**, *23* (26), 13040–13045. https://doi.org/10.1021/la702147m.

(51) Gritsch, S.; Nollert, P.; Jähnig, F.; Sackmann, E. Impedance Spectroscopy of Porin and Gramicidin Pores Reconstituted into Supported Lipid Bilayers on Indium−Tin-Oxide Electrodes. *Langmuir* **1998**, *14* (11), 3118–3125. https://doi.org/10.1021/la9710381.

(52) Steinem, C.; Janshoff, A.; Ulrich, W.-P.; Sieber, M.; Galla, H.-J. Impedance Analysis of Supported Lipid Bilayer Membranes: A Scrutiny of Different Preparation Techniques. *Biochim. Biophys. Acta BBA - Biomembr.* **1996**, *1279* (2), 169–180. https://doi.org/10.1016/0005-2736(95)00274-X.

(53) Lin, J.; Motylinski, J.; Krauson, A. J.; Wimley, W. C.; Searson, P. C.; Hristova, K. Interactions of Membrane Active Peptides with Planar Supported Bilayers: An Impedance Spectroscopy Study. *Langmuir* **2012**, *28* (14), 6088–6096. https://doi.org/10.1021/la300274n.

(54) Zhang Jing; Xie Xin; Zhou Xin; Chen Yu-Qing; Yu Ji-Cheng; Cao Guo-Ying; Wu Xiao-Jie; Shi Yao-Guo; Zhang Ying-Yuan. Permeability and Concentration of Levofloxacin in Epithelial Lining Fluid in Patients With Lower Respiratory Tract Infections. *J. Clin. Pharmacol.* **2013**, *50* (8), 922–928. https://doi.org/10.1177/0091270009355160.

(55) Deleu, M.; Crowet, J.-M.; Nasir, M. N.; Lins, L. Complementary Biophysical Tools to Investigate Lipid Specificity in the Interaction between Bioactive Molecules and the Plasma Membrane: A Review. *Biochim. Biophys. Acta BBA - Biomembr.* **2014**, *1838* (12), 3171–3190. https://doi.org/10.1016/j.bbamem.2014.08.023.

(56) Samelo, J.; Mora, M. J.; Granero, G. E.; Moreno, M. J. Partition of Amphiphilic Molecules to Lipid Bilayers by ITC: Low-Affinity Solutes. *ACS Omega* **2017**, *2* (10), 6863–6869. https://doi.org/10.1021/acsomega.7b01145.

(57) Oursel, D.; Loutelier-Bourhis, C.; Orange, N.; Chevalier, S.; Norris, V.; Lange, C. M. Lipid Composition of Membranes of Escherichia Coli by Liquid Chromatography/Tandem Mass Spectrometry Using Negative Electrospray Ionization. *Rapid Commun. Mass Spectrom.* **2007**, *21* (11), 1721–1728. https://doi.org/10.1002/rcm.3013.

(58) Mansy, S. S. Membrane Transport in Primitive Cells. *Cold Spring Harb. Perspect. Biol.* **2010**, *2* (8), a002188. https://doi.org/10.1101/cshperspect.a002188.

(59) Shinoda, W. Permeability across Lipid Membranes. *Biochim. Biophys. Acta BBA - Biomembr.* **2016**, *1858* (10), 2254–2265. https://doi.org/10.1016/j.bbamem.2016.03.032.

(60) Nguyen, T. T.; Conboy, J. C. High-Throughput Screening of Drug–Lipid Membrane Interactions via Counter-Propagating Second Harmonic Generation Imaging. *Anal. Chem.* **2011**, *83* (15), 5979–5988. https://doi.org/10.1021/ac2009614.

(61) Li, J.; Sun, J.; He, Z. Quantitative Structure–Retention Relationship Studies with Immobilized Artificial Membrane Chromatography: II: Partial Least Squares Regression. *J. Chromatogr. A* **2007**, *1140* (1–2), 174–179. https://doi.org/10.1016/j.chroma.2006.11.091.

(62) Yazdanian, M.; Briggs, K.; Jankovsky, C.; Hawi, A. The "High Solubility" Definition of the Current FDA Guidance on Biopharmaceutical Classification System May Be Too Strict for Acidic Drugs. *Pharm. Res.* **2004**, *21* (2), 293–299. https://doi.org/10.1023/B:PHAM.0000016242.48642.71.

(63) Lee, J. B.; Zgair, A.; Taha, D. A.; Zang, X.; Kagan, L.; Kim, T. H.; Kim, M. G.; Yun, H.; Fischer, P. M.; Gershkovich, P. Quantitative Analysis of Lab-to-Lab Variability in Caco-2 Permeability Assays. *Eur. J. Pharm. Biopharm.* **2017**, *114*, 38–42. https://doi.org/10.1016/j.ejpb.2016.12.027.

(64) Gonçalves, J. E.; Fernandes, M. B.; Chiann, C.; Gai, M. N.; Souza, J. D.; Storpirtis, S. Effect of PH, Mucin and Bovine Serum on Rifampicin Permeability through Caco-2 Cells. *Biopharm. Drug Dispos.* **2012**, *33* (6), 316–323. https://doi.org/10.1002/bdd.1802.

(65) Blokhina, S. V.; Sharapova, A. V.; Ol'khovich, M. V.; Volkova, T. V.; Perlovich, G. L. Solubility, Lipophilicity and Membrane Permeability of Some Fluoroquinolone Antimicrobials. *Eur. J. Pharm. Sci.* **2016**, *93*, 29–37. https://doi.org/10.1016/j.ejps.2016.07.016.

(66) Raiman, J.; Törmälehto, S.; Yritys, K.; Junginger, H. E.; Mönkkönen, J. Effects of Various Absorption Enhancers on Transport of Clodronate through Caco-2 Cells. *Int. J. Pharm.* **2003**, *261* (1), 129–136. https://doi.org/10.1016/S0378-5173(03)00300-4.

(67) Pereira-Leite, C.; Nunes, C.; Reis, S. Interaction of Nonsteroidal Anti-Inflammatory Drugs with Membranes: In Vitro Assessment and Relevance for Their Biological Actions. *Prog. Lipid Res.* **2013**, *52* (4), 571–584. https://doi.org/10.1016/j.plipres.2013.08.003.

(68) Nunes, C.; Brezesinski, G.; Pereira-Leite, C.; Lima, J. L. F. C.; Reis, S.; Lúcio, M. NSAIDs Interactions with Membranes: A Biophysical Approach. *Langmuir* **2011**, *27* (17), 10847–10858. https://doi.org/10.1021/la201600y.

(69) Nunes, C.; Lopes, D.; Pinheiro, M.; Pereira-Leite, C.; Reis, S. In Vitro Assessment of NSAIDs-Membrane Interactions: Significance for Pharmacological Actions. *Pharm. Res.* **2013**, *30* (8), 2097–2107. https://doi.org/10.1007/s11095-013-1066-8.

(70) Novakova, I.; Subileau, E.-A.; Toegel, S.; Gruber, D.; Lachmann, B.; Urban, E.; Chesne, C.; Noe, C. R.; Neuhaus, W. Transport Rankings of Non-Steroidal Antiinflammatory Drugs across Blood-Brain Barrier In Vitro Models. *PLOS ONE* **2014**, *9* (1), e86806. https://doi.org/10.1371/journal.pone.0086806.

(71) Suwalsky, M.; Manrique, M.; Villena, F.; Sotomayor, C. P. Structural Effects in Vitro of the Anti-Inflammatory Drug Diclofenac on Human Erythrocytes and Molecular Models of Cell Membranes. *Biophys. Chem.* **2009**, *141* (1), 34–40. https://doi.org/10.1016/j.bpc.2008.12.010.

(72) Moreno, M. M.; Garidel, P.; Suwalsky, M.; Howe, J.; Brandenburg, K. The Membrane-Activity of Ibuprofen, Diclofenac, and Naproxen: A Physico-Chemical Study with Lecithin Phospholipids. *Biochim. Biophys. Acta BBA - Biomembr.* **2009**, *1788* (6), 1296–1303. https://doi.org/10.1016/j.bbamem.2009.01.016.

(73) Lambri, M.; Dordoni, R.; Silva, A.; Faveri, D. M. D. Odor-Active Compound Adsorption onto Bentonite in a Model White Wine Solution. *Chem. Eng. Trans.* **2013**, 201–210. https://doi.org/10.3303/ACOS1311021.

(74) Rodrigues, C.; Gameiro, P.; Prieto, M.; de Castro, B. Interaction of Rifampicin and Isoniazid with Large Unilamellar Liposomes: Spectroscopic Location Studies. *Biochim. Biophys. Acta BBA - Gen. Subj.* **2003**, *1620* (1), 151–159. https://doi.org/10.1016/S0304-4165(02)00528-7.

(75) Pinheiro, M.; Pisco, S.; Silva, A. S.; Nunes, C.; Reis, S. Evaluation of the Effect of Rifampicin on the Biophysical Properties of the Membranes: Significance for Therapeutic and Side Effects. *Int. J. Pharm.* **2014**, *466* (1–2), 190–197. https://doi.org/10.1016/j.ijpharm.2014.03.005.

(76) Damodaran, K. V.; Merz, K. M. A Comparison of DMPC- and DLPE-Based Lipid Bilayers. *Biophys. J.* **1994**, *66* (4), 1076–1087. https://doi.org/10.1016/S0006-3495(94)80889-6.

(77) Leekumjorn, S.; Sum, A. K. Molecular Simulation Study of Structural and Dynamic Properties of Mixed DPPC/DPPE Bilayers. *Biophys. J.* **2006**, *90* (11), 3951–3965. https://doi.org/10.1529/biophysj.105.076596.

(78) Fernandes, F.; Neves, P.; Gameiro, P.; Loura, L. M. S.; Prieto, M. Ciprofloxacin Interactions with Bacterial Protein OmpF: Modelling of FRET from a Multi-Tryptophan Protein Trimer. *Biochim. Biophys. Acta BBA - Biomembr.* **2007**, *1768* (11), 2822–2830. https://doi.org/10.1016/j.bbamem.2007.07.016.

(79) Piddock, L. J. V.; Jin, Y.-F.; Ricci, V.; Asuquo, A. E. Quinolone Accumulation by Pseudomonas Aeruginosa, Staphylococcus Aureus and Escherichia Coli. *J. Antimicrob. Chemother.* **1999**, *43* (1), 61–70. https://doi.org/10.1093/jac/43.1.61.

(80) Ito, T.; Yano, I.; Tanaka, K.; Inui, K.-I. Transport of Quinolone Antibacterial Drugs by Human P-Glycoprotein Expressed in a Kidney Epithelial Cell Line, LLC-PK1. *J. Pharmacol. Exp. Ther.* **1997**, *282* (2), 955–960.

(81) Raiman, J.; Niemi, R.; Vepsäläinen, J.; Yritys, K.; Järvinen, T.; Mönkkönen, J. Effects of Calcium and Lipophilicity on Transport of Clodronate and Its Esters through Caco-2 Cells. *Int. J. Pharm.* **2001**, *213* (1), 135–142. https://doi.org/10.1016/S0378-5173(00)00655-4.

TOC graphics